Universidad de Zaragoza

Facultad de Ciencias

Departamento de Química Física

Fabrication of Hybrid Organic-Inorganic Electronic Molecular Devices

Fabricación de Dispositivos Electrónicos Moleculares Híbridos (Orgánicos-Inorgánicos)

Henrry Marcelo Osorio Calvopiña

Master's Degree Project

Zaragoza, September 2012

Universidad de Zaragoza

Departamento de Química Física

Instituto de Nanociencia de Aragón

PILAR CEA MINGUEZA, profesor titular del Departamento de Química Física y SANTIAGO MARTÍN SOLANS, contratado Ramón y Cajal del Departamento de Física de la Materia Condensada, de la Facultad de Ciencias de la Universidad de Zaragoza

CERTIFICAN:

Que el trabajo presentado en esta Memoria por D. Henrry Marcelo Osorio Calvopiña como Proyecto Final de Máster Universitario en Materiales Nanoestructurados para Aplicaciones Nanotecnológicas y que lleva por título "*Fabrication of Hybrid Organic-Inorganic Electronic Molecular Devices*", ha sido realizado en el Departamento de Química Física de la Facultad de Ciencias de la Universidad de Zaragoza, bajo la dirección de ambos, autorizando la presentación de la misma para su calificación por el tribunal correspondiente.

Y, para que así conste, expiden el presente documento en Zaragoza, a 3 de Septiembre de 2012.

Fdo: Pilar Cea Mingueza

Fdo: Santiago Martín Solans

ACKNOWLEDGEMENTS

I have taken efforts in this project. However, it would not have been possible without the kind support and help of many individuals and organizations. I would like to extend my sincere thanks to all of them.

In particular, I am very grateful to my supervisor, Dr. Pilar Cea who was abundantly helpful and offered invaluable assistance, support and guidance.

I would like to gratefully acknowledge the enthusiastic supervision of Dr. Santiago Martín during this work.

I thank to the PLATON research group for sharing the literature and invaluable assistance.

I am very grateful the financial assistance corresponding to the SENESCYT GRANT, financed by Secretaría Nacional de Educación Superior, Ciencia, Tecnología e Innovación (SENESCYT) from Government of Ecuador.

I also thank the Department of Physical Chemistry at the University of Zaragoza, the Advanced Microscopy Laboratory (LMA) and the Institute of Nanoscience of Aragon (INA) the ability to use their infrastructure.

INDEX

1. INTRODUCTION 5

2. MOLECULAR ASSEMBLY TECHNIQUES: LANGMUIR-BLODGETT AND SELF ASSEMBLY 11

2.1. Langmuir-Blodgett Technique 11

2.1.1. Langmuir Films 11

2.1.2. Langmuir-Blodgett Films 16

2.2. Self – Assembly technique 17

3. EXPERIMENTAL SECTION 20

3.1. Preparation of Langmuir films 20

3.1.1 Langmuir Trough 20

3.2. Langmuir films Characterization 22

3.2.1. Surface potential 22

3.2.2. Brewster Angle Microscopy (BAM) 23

3.3. LAngmuir-Blodgett films characterization 25

3.3.1. Quartz crystal microbalance (QCM) 25

3.3.2. UV-vis Spectroscopy 26

3.3.3. Cyclic voltammetry (CV) 27

3.3.4. Atomic force microscopy (AFM) 30

3.4. Single molecule Conductance 31

3.4.1. STM-Break junction technique 32

3.4.2. *I(s)* technique 32

4. STUDY AND CHARACTERIZATION OF LANGMUIR AND LANGMUIR-BLODGETT FILMS INCORPORATING AN ORGANOMETALLIC COMPOUND. 35

4.1. Langmuir Films 35

4.2. Langmuir-Blodgett Films 38

4.3. Mixed Langmuir films of *TMS-Ru-TMS* and *TMS-OPE-NH_3Cl* 43

4.4. Self-assembly films 47

4.5. Single Molecule Conductance for *TMS-Ru-TMS* and *TMS-OPE-TMS* 49

CONCLUSIONS 52

REFERENCES 54

1. INTRODUCTION

Molecular electronics defined as "making an information processing device with a single molecule or small number of assembled molecules" becomes increasingly investigated and envisioned as a promising candidate for the nanoelectronic of the future [1-2]. Molecular nanostructures have been particularly attractive because of interest in both investigations of fundamental physical properties and potential applications in next-generation electronic devices [3-5]. Some of these applications are memory devices [6-12], rectifier diodes [2], electrical insulators [13] and/or molecular wires.

In the case of memory devices, the physical property used is the bistability that occurs when the free energy of the system has two minima "equilibrium states" separated by a maximum [6-8]. Experimentally memory devices for its study are building through two main structures: organic|inorganic|organic tree layered system [9, 12] and composites of conducting polymers [10, 14]. There are several theories for explaining bistable behavior, one of them is proposed by Colle et al. [15], in which proposes that switching is due to the oxide layer at the electrode and transport through filaments.

For rectifier diodes, the system used for Voltage-Current study is Si|molecule|metal junctions. According to Lenfant et al. [2] the Fermi-level at the π group|metal interface is mainly responsible for the rectifier behavior.

Finally, the study of molecular conductance junctions gives the electrical insulator or molecular wire behavior. The molecular conductance junction is a structure in which single molecule or small groups of molecules conduct electrical current between two electrodes [16], if this conductance is high a molecular wire is obtained, but if the conductance is suppressed an insulator would be obtained. Nakamura et al. [13] have shown by first time that ditelluride monolayers are formed on the surfaces due to the autooxidation of the ditelluride even when these monolayers have high resistance.

In all discussed applications, electron transfer at the molecule-metal interface is important [17-19] and there are several theoretical and experimental studies made. From the theoretical point of view, the two most relevant challenges are the relative alignment of the molecular states respect to the metal Fermi-level (E_F) and the work function (Φ) of the

covered metal electrode [19-25]. Experimentally, the electron transfer is governed by the tail and the anchorage group of the molecule [2, 18, 26-34], both related with the theoretical quantities (E_F and Φ) when molecule is anchored to the metal substrate [2, 18-19, 27].

From the experimental point of view, substrates which can be used could be Au, Ag, Pt, Ni, SiO_2, etc [20, 25, 35]. Although the most used is gold mainly because: the most of the conductance measurements uses gold substrates coated with molecules via Self-Assembly (SA) technique [36]; gold is easy to obtain, both as a thin film and a colloid; is exceptionally easy to pattern by a combination of lithographic tools and chemical etchants; is a reasonably inert metal; thin films of gold are common substrates used for a number of spectroscopy and analytical techniques; and because in biological applications, gold is compatible with cells.

Thus, state-of-the-art is focused on the design, synthesis of molecules and conductance measure of molecule-metal junctions. As mentioned above, the main parts of the molecule for electron transmission are the tail and the anchorage group (terminal group). It is demonstrated that if the head group is on the far side of the molecule only changes the Self-Assembled monolayers (SAMs) local electrostatic potential on that side of the layer [20]. Therefore, the efforts in researching are involved in the molecular design with tail and anchorage groups, which offer a good molecule-metal bonding and a good electron transmission.

In molecular electronic, the electron transport along a single molecule, overall π-conjugated molecules, on noble metal electrodes are being used [17, 20-21]. In order to obtain a delocalized π-electron system several molecules with different tails have been studied, the most studied are conjugated thiols [1-2, 17, 21, 23, 37], bypiridine systems [29, 32-34], olygoyne systems [31], or phenyl systems [35, 38]. A special particularity was found, practically all molecular wires obey a length-dependent charge transport rule revealing that an energy mismatch between the molecular orbitals and electrode Fermi-level is originated, which is a problem in long-range electron transport [38]. Taking in account this problem, it has been reported in the literature [31] that olygoynes are weakly dependent on the molecular length, in contrast to some phenyl systems, specifically oligo

(phenyleneethynylene) derivatives, (OPEs) [i.e., $(C_6H_4 - C \equiv C-)_n$] oligo (phenylenevinylene) derivatives, (OPVs) [i.e., $(C_6H_4 - CH = CH-)_n$]

Nevertheless, there are several advantages in using OPEs in molecular electronics due to have a rigid molecular structure and an extended delocalized π-electron system. The conjugated backbone and the rigid-rod structure facilitate wire-like properties and, in addition, this class of oligomers can behave as real full current controllers because the electronic transport properties vary significantly depending on molecular conformations [39]. For these reason OPEs are being studied, and to overcome the length-dependent charge transport, the incorporation of metal atoms to the π-conjugated backbone is being proposed [38] and the reported results are successful.

In the same way, to improve the electron transport in molecule-metal junctions, the interaction metal-molecule along the anchoring group of the molecule has to be understood. There are two main characteristics that have to present an anchoring group in order to be considerate in molecular electronic. Firstly, produce a strong molecule-metal bond, which leads to the effective hybridization of the molecular and metal orbitals [18]. Secondly, generate a smaller energy difference between the Fermi-level of the metal electrode and the conduction orbital of the molecule [17-18]. Taking in account these mentioned characteristics, the most studied anchoring group reported in the literature is the thiol ($-SH$) [1, 17, 21-24, 35], since the gold-sulfur bond is strong and this bond is very used in SAMs [18, 27].

In order to improve the conduction minimizing the difference in the Fermi-level of the metal and molecule, the use of new anchorage groups which can form more stable and higher metal-molecule junctions are required [18, 27]. Recent studies report the use of new anchoring groups such as: selenol ($-SeH$) [19-20, 27-28, 40-42], isocyanide ($-NC$) [18, 25-26], and pyridine [29-34], etc.

In the case of selenol, according to Yokota et al. [19, 27] the Au-Se bond is metallic and it is predicted to be able to reduce the device operating voltages. Shaporenko et al. [28] showed that selenol is better than thiol presumably because selenolates have better ability to adjust the surface lattice of the substrate to the most favorable 2D arrangement of the

adsorbate molecules. In both studies, the conclusion is that selenol anchoring group improves the electron transfer in the molecule-metal junction and it is concluded that Au-Se interface is more appropriate for molecular devices than Au-S interface.

In the case of isocyanide, according to Kiguchi et al. [18] the strength of the metal-CN bond is comparable to that of the metal-S bond and this strong bond may contribute to increase the electron transport in the molecule-metal junction. The study shows that the conductance of the molecular junction with Au-CN bond is comparable to that of the molecular junction with the Au-S bond. This result is in agreement with the work of Seminario et al. [25], and it is conclude that isocyanide anchoring group is a promising alternative to the thiol.

In the case of pyridine, it is showed its good behavior like anchoring group [20], but this group is actually important because influences in the molecule modifying the electron transport properties of π-conjugated systems [29]. Pyridine produces that the molecule presents several conductance values [29, 31-33]. According to Wang et al. [31] the high conductance value is due to the adsorption of the pyridyl group at more highly coordinated sites such as steps edges or alongside gold adatoms, and according to Kamenetska et al. the lower conductance value occurs when the Au-N donor-acceptor bond is along the molecular backbone [33]. Several studies have shown that different anchoring geometries produce different conductance values [31-32] dictated preliminary by the separation between electrodes [34]. This behavior is important because it could be the basis of a new class of mechanically activated single-molecule switches [32].

Thus, the present work is an input in the field of molecular electronic focus on the conductance along molecule-metal junctions. Compounds showed in Figure 1.1 were studied and present two fundamental characteristics: are OPE derivatives, being good candidates for electron transmission as has been said; and present a new anchoring group, trimethylsilane (TMS), which has been reported [43] to offer a good anchorage between molecule and substrate and present a good conductance. In the present work, *TMS-Ru-TMS* (Figure 1.1A) is analyzed in more detail because incorporates a ruthenium atom in the π-conjugated backbone, and it is reported [38] that this particularity improves the conductance behavior.

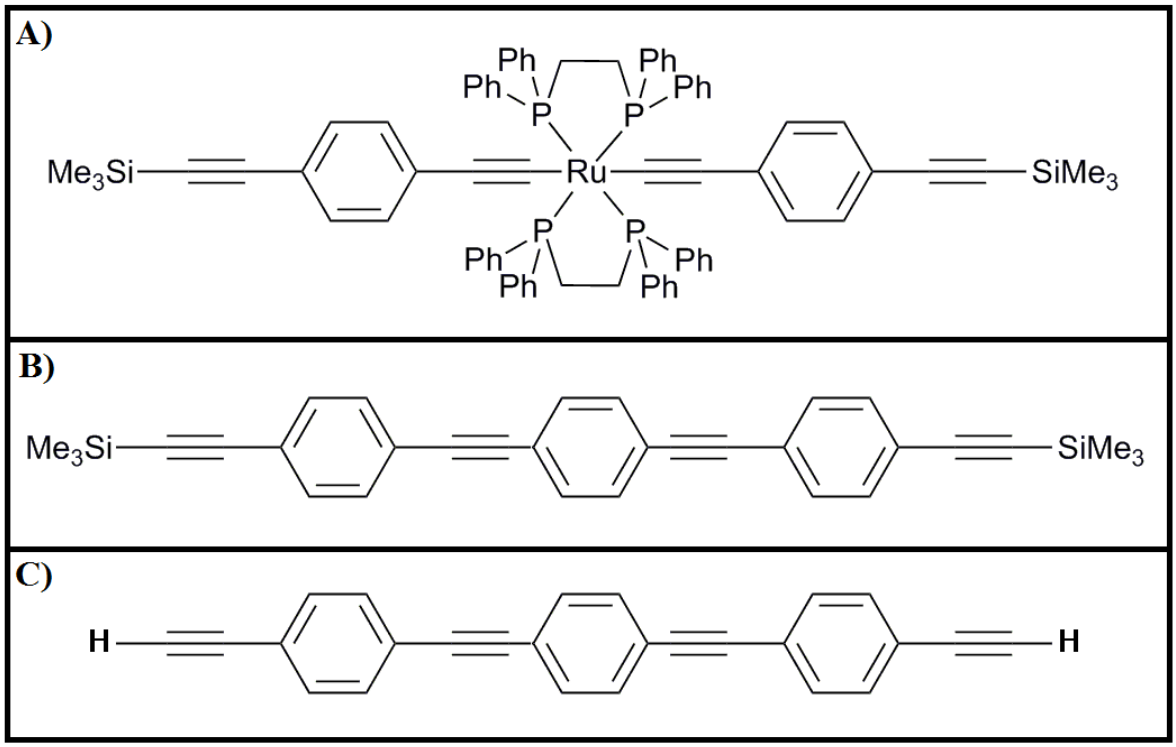

Figure 1.1. *Structures of studied molecules in this work. A)* $trans - Ru(-C \equiv C - C_6H_4 - C \equiv C - SiMe_3 - 4)_2(dppe)_2$ *, (TMS-Ru-TMS). B) 1, 4-bis((4-((trimethylsilyl)ethynyl)phenyl)ethynyl)benzene, (TMS-OPE-TMS). C) 1,4-bis(4-ethynylphenyl)ethynyl)benzene, (HC2-OPE-C2H).*

Therefore, the main objectives of this work are:

- Fabricate well-ordered molecule monolayer-metal systems incorporating materials with potential applications in molecular electronic.

- Characterize the electrical properties in isolated molecule systems; and compare the results produced by different molecules to determine the effect of each component in the conductance along the molecule and molecule-metal junction.

In particular, the tasks to be developed are:

- Find the best conditions in order to obtain well-ordered films. The molecules will be incorporated into the metal substrate by Self-Assembly and Langmuir-Blodgett techniques.

- Characterization of the monomolecular films using a wide range of optical, electrochemical, spectroscopic and scanning probe techniques to determine the molecular arrangement of the material in the films.

- Determine the electrical properties, in particular, in single molecule systems.

2. MOLECULAR ASSEMBLY TECHNIQUES: LANGMUIR-BLODGETT AND SELF ASSEMBLY

2.1. LANGMUIR-BLODGETT TECHNIQUE

The Langmuir-Blodgett (LB) technique is a bottom-up and room-temperature deposition process that may be used to deposit mono and multilayered films of organic materials. Furthermore, this method permits the manipulation of organic molecules on the nanometer scale, thereby allowing intriguing super-lattice architectures to be assembled. The generation of these films has two main parts, first the formation of Langmuir films in the air-water interphase and after the transference of these films to the substrate [1-3, 39, 44-47].

2.1.1. Langmuir Films

The formation of Langmuir films is based on the deposition of the molecules under study on the liquid surface (usually water or an aqueous solution) resulting in a film of monomolecular thickness. Molecules which form monolayers at the air-water interface have an amphiphilic structure, i.e. with a hydrophobic portion, usually constituted by one or more aliphatic chains that prevent its solubilization in the subphase providing the interactions between neighboring molecules necessary to stabilize the monolayer formed, and a hydrophilic portion containing polar functional group/s that allow the anchorage of the amphiphilic material at the water surface and, therefore, stable film formation on the air-water interface. These types of molecules have the capacity to self-organize on a liquid surface when their available space is decreased by a moving barrier, forming an orderly monolayer or Langmuir film.

The preparation of these Langmuir monolayers or films is carried out in a device called Langmuir trough, which essentially is a Teflon container filled with water (or an aqueous solution) on which the studied molecules will be spread. The main components of the Langmuir trough are: a device to measure the surface pressure (usually a Wilhelmy balance), a movable barrier which compresses the film and a vertical dipper that holds the

solid supports to carry out the transfer. Figure 2.1 shows a photograph of a Langmuir trough where the main components are shown.

Figure 2.1. *KSV Commercial Langmuir trough. A) Wilhelmy balance. B) Dipper. C) Mobile barriers [47].*

The first step to obtain a Langmuir film is the preparation of an organic and diluted solution of a very well-known concentration of the molecule under study. The solvent or solvent mixture, used to dissolve the material, should be insoluble in water, it should not form complexes or react with the molecule, and it must have a high volatility [48].

With the aid of a micropipette or syringe, a known volume of the organic solution is spread on the water surface. The way in which the spreading process of the molecules is carried out is one of the factors that determine the quality of the monolayers at the air-water. The dispersion should be made by slowly spreading the solution drop by drop at a distance as close as possible to the water surface favoring that the repulsive forces between the solvent and water overcomes gravitational forces, and thereby the drop remains on the surface. The drops must be homogeneously distributed on the water surface to avoid the formation of aggregates which prevent the formation of good monolayers. After the spreading process of a drop it is convenient to wait some time before the next drop is spread to allow evaporation of the solvent and promote the molecules diffusion on the water surface. Figure 2.2A shows a scheme of the spreading process.

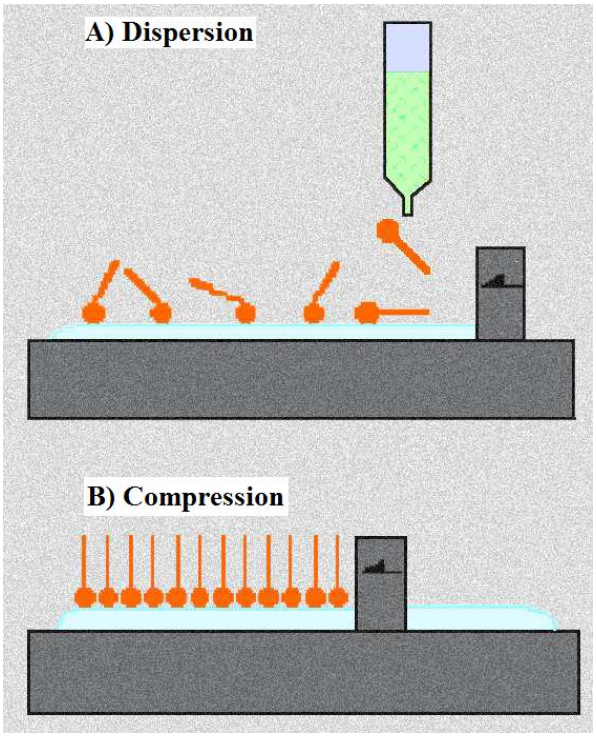

Figure 2.2. *A) Spreading process. B) Compression process [47].*

After waiting approximately fifteen minutes to allow the complete evaporation of the solvent, the compression process begins. This process consists in the reduction of the available physical space in the water surface for the molecules; the compression is carried out with a slow movement of the mobile barrier and the molecules begin to approach. As a result, the molecules begin to interact between them and gradually an ordered film is obtained at the air-water interface. Figure 2.2B shows a scheme of the compression process. Under these circumstances the system has a surface tension (γ) lower than the clean water surface (in the absence of a monolayer) (γ_0). Upon the compression process, in which the temperature remains constant, the surface tension decreases and the surface pressure (π) is then defined as [47]:

$$\pi = \gamma_0 - \gamma \qquad (2.1)$$

The measurement of the surface tension is usually performed by a Wilhelmy balance [49]. This method makes use of a thin sheet (usually aluminum, platinum or filter paper) that is suspended from a sensor and partially introduced into the aqueous subphase. Three main forces act on this sheet: gravity, surface tension and the upward buoyant force

[50]. Among them, the only force which is influenced by the presence of the monolayer on the surface is the surface tension. Therefore, the potential difference which indicates the sensor before and after spreading the organic material on the water surface is due to the change in surface tension between the clean surface and the surface with monolayer, as defined in equation 2.1, the surface pressure.

The graph that represents the surface pressure versus the area per molecule, recorded at constant temperature, is known as compression isotherm or surface pressure-area isotherm (π-*A*) [51]. This isotherm is different for each molecule and the conditions under which it was obtained. π-*A* isotherms provide information about the stability of the monolayer at the air-water interface, the organization of the molecules in the film and the phase and phase transitions of the monolayer upon the compression process. Figure 2.3 shows a scheme of an isotherm showing all the phase and phase transitions that have been described in the literature. It is important to note that not all compounds show all these phase and phase transitions [52].

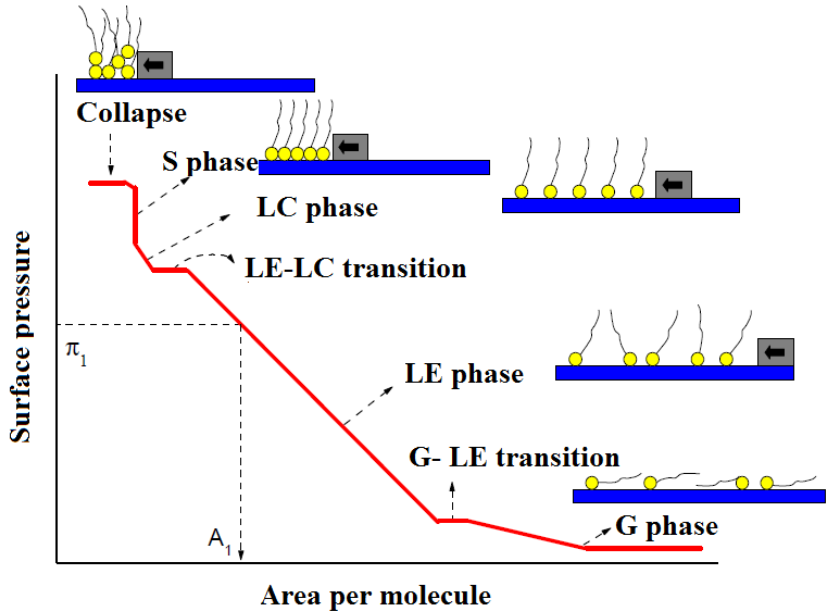

Figure 2.3. *Scheme of a surface pressure vs. area per molecule isotherm where* A_1 *represents the area per molecule at given surface pressure* (π_1) *[47].*

Gas phase (G). At the beginning of compression the distance between molecules is considerable, the available area is much larger than molecular dimensions and molecular

interactions are small. Under these conditions the material deposited on the water surface has relatively little effect on the surface tension of water and thus the surface pressure is closed to zero.

Gas - liquid expanded transition (G-LE). When the available area per molecule decreases, there is a slight but gradual increase in the surface pressure until it reaches a *plateau* or horizontal region in which the hydrophobic chains, initially located near the water surface, begin to rise. This point corresponds to the transition from gas to liquid, at this point there is a coexistence of two phases.

Liquid expanded phase (LE). At the end of the *plateau* there is a very fluid phase that is quite compressible, in which the interactions between chains of the molecules become larger as they get closer. This is the so-called liquid expanded phase. Therefore, in this LE phase the molecules undergo significant attraction forces.

Liquid expanded-liquid condensed transition (LE-LC). Again, this phase transition is characterized by the appearance of a *plateau* in the isotherm that determines the appearance of the liquid condensed phase.

Condensed liquid phase (LC). A change in slope indicates the presence of a new phase named condensed liquid phase, where the molecules are more compactly packed and the hydrophobic chains are located vertically, further from the aqueous surface. In this phase the attractive interactions between the molecules begin to be significant, leading to a close packing between them, which gives rise to a long distance orientational order. In addition, the compressibility of the monolayer is relatively low.

Solid phase (S). If the area per molecule continues to decrease, the molecules are close to their neighbors resulting in an arrangement known as solid phase in which the available area per molecule corresponds to the molecular section. Molecules reach a high degree of ordering with hydrophobic chains being well-packed thanks to the strong interactions between them. The compressibility of the film is very low.

Collapse. The collapse of the monolayer occurs when an area per molecule smaller than the molecule cross section is reached. At this point a multilayered film is formed (most

of time a disordered multilayered film). The collapse surface pressure of the monolayer depends on several factors including temperature, the compression speed, the nature of the material and the nature of the subphase [52-53].

2.1.2. Langmuir-Blodgett Films

After a stable monolayer at the air-water interface has been obtained, it can be transferred to a solid substrate, leading to the formation of a Langmuir-Blodgett film (LB film).

The transfer process consists in a slow vertical motion of the dipper holding the solid support in the order of a few millimeters per minute, and then the molecules are deposited on the solid. The transference is carried out at a constant surface pressure, determined experimentally, as the most appropriate surface pressure of transference which depends on the nature of the monolayer. This deposition is performed at a surface pressure of transference below the collapse surface pressure, which ensures the deposition of monolayers in the substrate, preventing the generation and deposition of multilayers. Figure 2.4 shows the transference process.

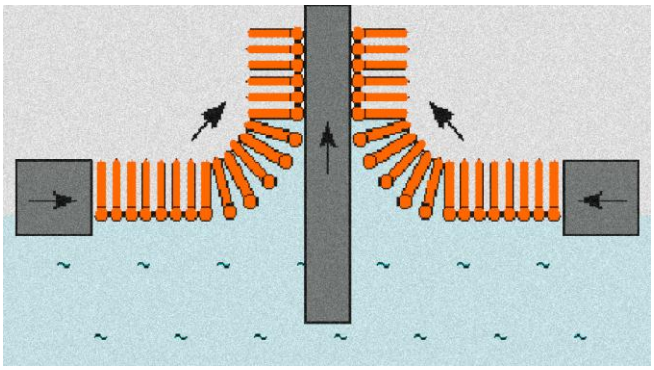

Figure 2.4. *Transference of a Langmuir film onto a solid surface [47].*

For the transference process to take place it is necessary that the forces of interaction between the Langmuir film and the substrate are greater than the forces of interaction between the film and the aqueous surface. Thus, if the substrate has a hydrophilic nature, the transfer will occur during the emersion of the substrate, then the polar heads of the molecules composing the film remain attached to the support. However,

when the substrate has a hydrophobic nature, it is the hydrophobic part of the molecule the one that will interact with the solid, resulting in the deposition during the immersion of the substrate into the aqueous subphase. Depending on the nature of the molecule under study, three different types of transfers: Y, X and Z can be produced. These types of geometries are shown in Figure 2.5.

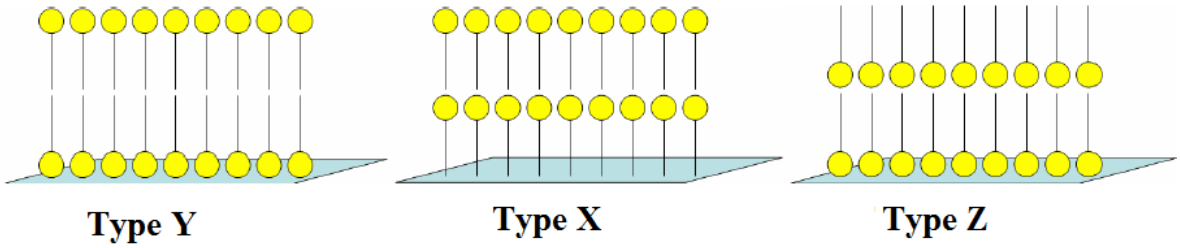

Figure 2.5. *Different geometries that can be obtained in the transference of Langmuir Films on a solid substrate, each one depends of the nature of the substrate [47].*

LB technique has many advantages over other techniques. Taking in account other useful liquid deposition technique, Self-assembly (SA), LB allows deposition of molecules by means of chemisorption and physisorption, while the molecular assembly in SA is performed only by chemisorption. Also, as mentioned LB allows having good control in the order of the molecules and the deposition of several ordered layers over the substrate.

2.2. SELF – ASSEMBLY TECHNIQUE

Self-assembly (SA) monolayers (SAM) are molecular assemblies that are formed spontaneously by the immersion of an appropriated substrate into a solution of an active surfactant in an organic solvent [39]. There are several types of SA methods that yield organic monolayers. Meanwhile LB films are more difficult to prepare and are not sufficiently mechanically stable for most purposes, SA are stronger, are easier to fabricate, and make use of a great variety of available starting materials. The main limitation in SA films is the need of a chemical reaction between one functional group in the molecule with the substrate to produce chemisorbed films. Once the route and optimum conditions to

fabricate a self-assembly film are known, it is easy and cheap to produce a monomolecular layers. However, long and detailed studies are normally needed to find such procedure.

SA monolayers have been prepared on various metallic and inorganic substrates such as Ag, Au, Cu, Ge, Pt, Si, GaAs, SiO_2, and many other materials; although gold is one of the most widely substrates employed. From the thermodynamically point of view, a self-assembly surfactant molecule can be divided into three parts as are shown in Figure 2.6. The first part is the head group that provides the most exothermic process, i.e., chemisorption on the substrate surface. The very strong molecular-substrate interactions result in an apparent pinning of the head group to a specific site on the surface through a chemical bond (covalent; covalent but slightly polar; ionic). The energies associated with the chemisorption are at the order of tens of $kcal \cdot mol^{-1}$. As a result of the exothermic head group-substrate interactions, molecules try to occupy every available binding site on the surface, and in this process interactions push together molecules that have already being adsorbed.

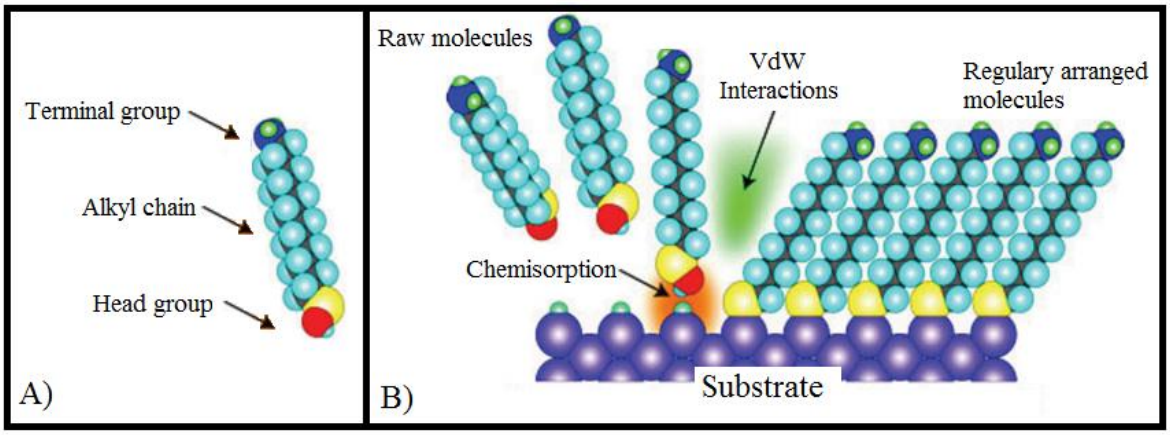

Figure 2.6. *A) Surfactant molecule parts. B) Scheme of Self-assembly process [54].*

This implies that some surface mobility prior to final pinning has to be assumed; otherwise the formation of crystalline molecular assemblies cannot be explained. The chemisorption exothermicity may be compared, in principle, to the pressure that the barrier in a Langmuir trough applies to the amphiphilic molecules at the air-water interface. It is this spontaneous molecular adsorption that brings molecules close enough together and

allows for the short-range, dispersive, London-type, van der Waals forces to become important. During this process a real new chemical bond is formed.

The second molecular part is the alkyl chain, and the energies associated with its inter-chain van der Waals interactions are at the order of 10 kcal/mol, i.e., it is an exothermic process. It is necessary to note here that self-assembly of amphiphilic hydrocarbon molecules cannot be possible taking in account only the interactions among the alkyl chains. Thus, it should bear in mind that the first and most important process in a SA process is chemisorption. Only when molecules are put in a correct place on the surface, the formation of an ordered and closely packed assembly starts; although, Van der Waals interactions are the main forces in the case of simple alkyl chains. On the other hand, when a polar bulky group is substituted into the alkyl chain, there are also long-range electrostatic interactions that, in some cases, are energetically more important than van der Waals attractions.

The third molecular part is a terminal functionality group, which, in the case of a simple alkyl chain, is a methyl group. These surface groups are thermally disordered at room temperature.

To prepare a self-assembly monolayer, firstly it is necessary to select the organic solvent to prepare the solution (1 - 10 mM) of the compound; the common used solvent is ethanol, although other ones also can be used such as chloroform, tetrahydrofuran, acetonitrile, toluene, etc. Once the solvent is selected, the film construction is performed by immersing a clean substrate into the dilute solution by an approximate time of 24 hours at room temperature. The amount of deposited molecule can be controlled making use of a Quartz Crystal Microbalance which allows calculating the mass deposited on the substrate by the frequency variation recorded before and after the immersion of the substrate. After this deposition time, a cleaning process of the substrate is needed to remove the physisorbed molecules in the surface washing the substrate with the same solvent used to prepare the solution and drying with a flow of N_2. In the case of gold substrates, they must be heated before being used. During this flame annealing process, the slide took on a slight orange hue and it is kept in this state for around 60 seconds. This procedure is known to result in atomically flat Au(111) terraces.

3. EXPERIMENTAL SECTION

3.1. PREPARATION OF LANGMUIR FILMS

3.1.1 Langmuir Trough

For the realization of this work 2 Langmuir troughs of the laboratory at the Physical Chemistry Laboratory of the University of Zaragoza were used. One of them is a NIMA trough, model 702, and the second one is a KSV, model 5000.

The NIMA trough, shown in Figure 3.1, has dimensions 100 x 720 mm². This trough has been used to record the surface pressure and surface potential vs. area per molecule isotherms, the UV-vis reflection spectroscopy and the Brewster angle microscopy experiments. The trough is made of Teflon and it has two movable barriers. Surface pressure measurements are carried out with a Wilhelmy balance, which is located in the center of the trough.

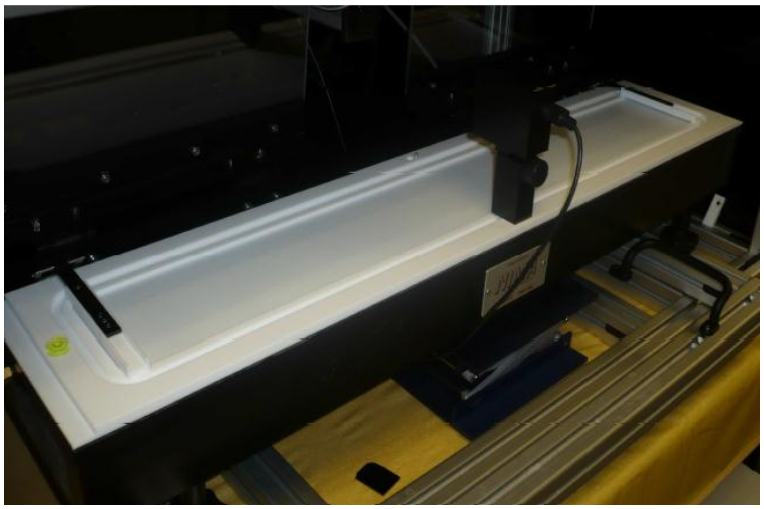

Figure 3.1. *NIMA trough, model 702 [47].*

The KSV trough, shown in Figure 3.2, consists of two containers of dimensions 120 x 775 mm² each, giving a total effective area of 240 x 775 nm². The two containers are also made of Teflon and they have two movable barriers. The main feature of this through is the presence of these two containers and a third one in the middle (just containing the pure

water subphase) which allows the formation of alternating Langmuir-Blodgett films. Surface pressure measurements are performed with the Wilhelmy balance, which is located in the center of through. The equipment consists of a vertical dipper that allows the deposition of Langmuir films on a solid substrate. This trough has been used to fabricate the LB films reported in this dissertation.

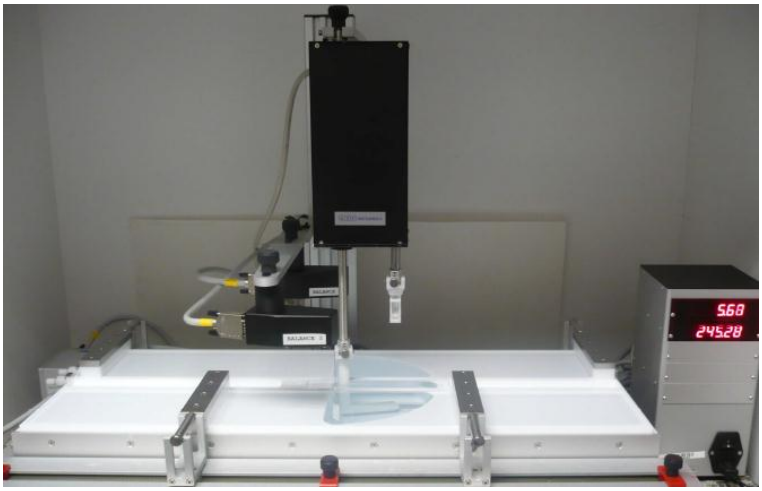

Figure 3.2. *KSV trough, model 5000 [47].*

These troughs are housed in a constant temperature (20 ± 1 ° C) cleaned room. To achieve a clean environment in the laboratory, the lab has two doors and a perfectly sealed window. Furthermore, in order to minimize possible contamination, the researchers must wear a clean lab coat, pants and gloves. All the material that enters the lab has to be carefully cleaned with ethanol in order to remove grease traces and dust. The cleaning of the lab is done daily by researchers working on it [39, 47]. Finally, the Langmuir troughs are in closed glass cases to avoid, as far as possible the presence of impurities that might affect the results.

3.2. LANGMUIR FILMS CHARACTERIZATION

3.2.1. Surface potential

Measurements of surface potential of the monolayer on the water surface were performed using the Kelvin Probe SP1 equipment by Nanofilm (Göttingen, Germany), which operates with the vibrating plate method. The equipment is shown in Figure 3.3.

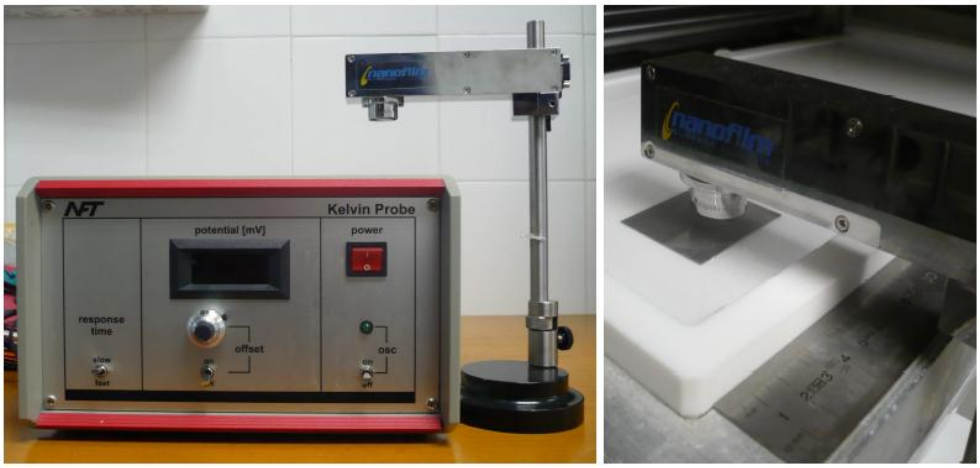

Figure 3.3. *Kelvin Probe SP1 instrument provided by Nanofilm for surface potential vs. area per molecule measurements [47].*

The method of the vibrating plate is based in the measure of the capacitance in the capacitor formed between two electrodes, arranged one at the bottom of the Langmuir trough (a rectangular sheet of stainless steel) and other electrode outside, a few millimeters above the water surface (a circular sheet of platinum of 15 mm in diameter). The electrode located outside of the subphase oscillates with a frequency of 200 Hz, generating an alternating current in the capacitor, which then can be amplified and detected. The Kelvin probe equipment detects the alternating current with the oscillator signal, and an electric circuit generates a current feedback compensatory then the potential inside the condenser is set to zero when the subphase is cleaned, before the dispersion of the molecule under study. Thus, the computer can record the potential differences upon the compression process [56]. Figure 3.4 shows a diagram of operation of the surface potential Kelvin probe system used in this work.

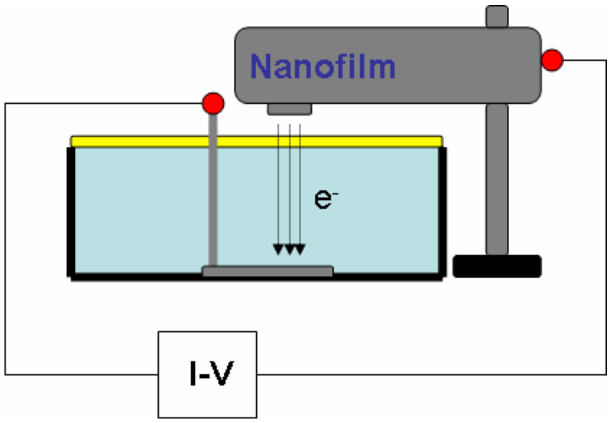

Figure 3.4. *Representative diagram of the operation in the surface potential measurements [47].*

The air-water interface is polarized as a result of spontaneous orientation of the water molecules in their vicinity. This polarization produces a surface potential at the interface which can be modified by the presence of an insoluble monolayer. It is therefore possible to measure the surface potential change when there is an insoluble monolayer in the interface with respect to the clean water. Detected changes should not be only attributed to the presence of the monolayer, but also depend on the reorientation of the dipoles of water and the specific adsorption of ions with the corresponding formation of the ionic double layer. It is therefore possible to estimate the surface dipole moment and consequently, orientation of the molecules at the interface by measuring the surface potential and knowing the area occupied by one molecule. Another important application of the surface potential is that it allows observing the heterogeneities in the monolayer due to the appearance of erratic fluctuations [57-58].

3.2.2. Brewster Angle Microscopy (BAM)

Images of Brewster angle microscopy were recorded with a mini-BAM of Nanofilm (Göttingen, Germany). A photograph of this instrument is shown in Figure 3.5.

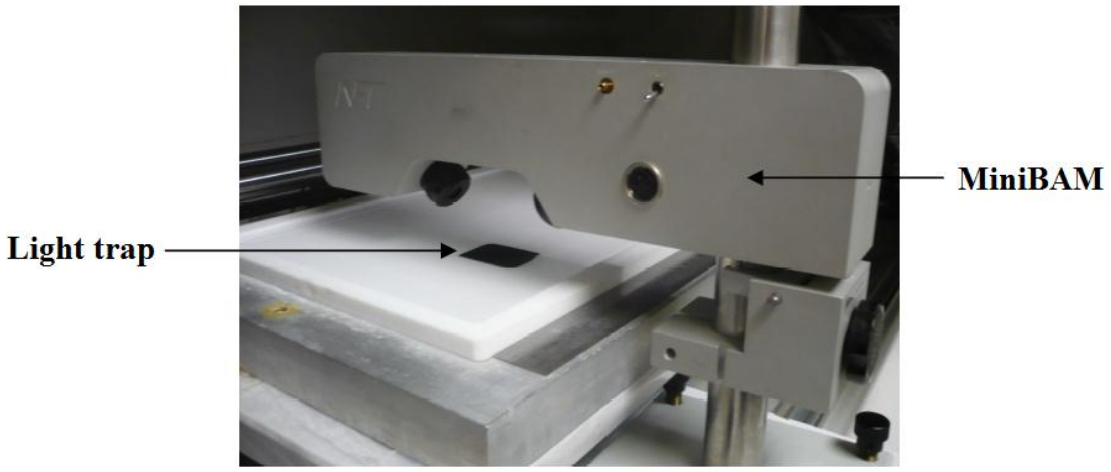

Figure 3.5. *Mini-BAM from Nanofilm [47].*

The physical principle of the performance of this technique is as follows: when a beam of polarized light (*p*-polarized) falls on the air-water interface with an angle of incidence equal to the Brewster angle (i), reflection is not produced and all light is transmitted. The Brewster angle is defined in equation 3.1. However, if an organic material is spread at the air-water interface, the refractive index of the aqueous subphase is modified by the presence of the film. Therefore, if the original angle of incidence is kept constant the Brewster angle condition is not maintained, so a small part of the incident light beam is reflected. This reflected beam is captured by a detector that converts the signal to a bitmap image. The fundamentals of this microscopy are shown in Figure 3.6. The incident beam used is a red laser (30 mW, 688 nm) and the lateral resolution of the optical system in the surface water plane is less than 20 µm. Brewster angle microscopy provides information about the formation of the monolayer at the air-water interface and it can detect the presence of aggregates during the three-dimensional or multi-layer film formation [47, 58].

$$\tan i = \frac{n_2}{n_1} \qquad (3.1)$$

where i is the Brewster angle, n_1 and n_2 are the refraction index of air and water, respectively.

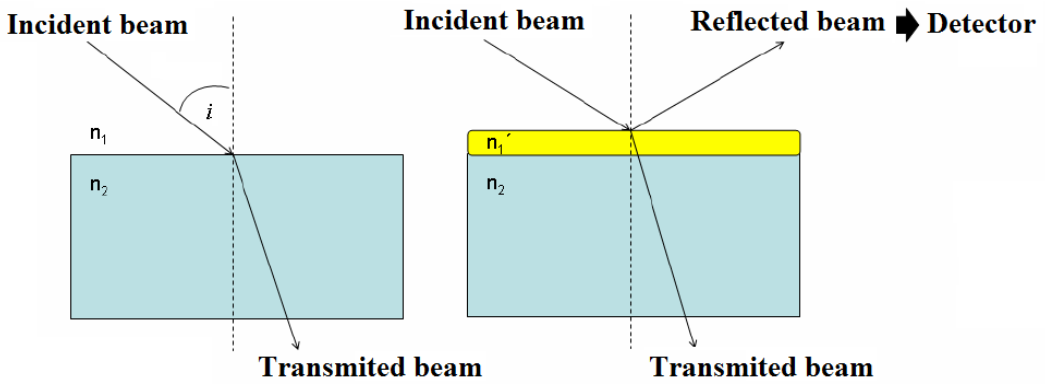

Figure 3.6. *Scheme of Brewster angle microscopy [47].*

3.3. LANGMUIR-BLODGETT FILMS CHARACTERIZATION

3.3.1. Quartz crystal microbalance (QCM)

The quartz crystal microbalance used in this work is a model QCM200 that operates with a QCM25 sensor of the commercial Stanford Research Systems. The microbalance and the sensor are shown in Figure 3.7. The sensor is a thin disk of α-quartz, with a thickness of about 331 µm, which is cut in the direction AT (35° 15'). The circular disc presents gold electrodes on both sides and its nominal frequency of oscillation is ca. 5 MHz. The front electrode area is ~1.37 cm², however, the oscillation active of the electrode is reduced to the overlap area of both circular electrodes ~ 0.40 cm².

The application of an oscillating electric field of appropriate frequency between the sensor electrodes induces an oscillation in the crystal, which propagates through the quartz with a movement of the disk surface parallel to the face of it. The maximum displacement takes place on both sides of the glass, and then the device is sensitive to disturbances that occur in the surface such as the deposition of a film. The variation in mass per unit area in the quartz glass is related to the variation in the oscillation frequency of the crystal according to the Sauerbrey equation [59] presented in equation 3.2.

Figure 3.7. *A) Quartz crystal microbalance model QCM200. B) QCM25 sensor [47].*

$$\Delta f = -C_f . \Delta m \qquad (3.2)$$

where Δf is the frequency variation measured with the QCM, Δm is the mass variation and C_f is the quartz sensitivity factor.

3.3.2. UV-vis Spectroscopy

UV-vis absorption spectroscopy was obtained with a commercial spectrophotometer Varian Cary 50 Bio UV-vis. The equipment is shown in Figure 3.8.

Figure 3.8.*Varian Cary 50 Bio UV-vis spectrophotometer [47].*

The principle of UV-vis absorption spectroscopy involves the absorption of radiation in the ultraviolet-visible provided by the molecule. This absorption of radiation is due to the promotion of electrons in the orbitals of lowest energy to highest energy orbitals, resulting in an excited electronic state. When the incident beam intensity (I_0) goes through the sample containing the analyte absorbent, it is attenuated to the transmitted beam intensity (I). Thus, the fraction which has been transferred is called the sample transmittance (T) [47].The relationship between transmittance and absorbance is illustrated in Equation 3.3.

$$A = -\log\left(\frac{I}{I_0}\right) = -\log(T) \qquad (3.3)$$

This technique has been used to characterize both the molecules in solution and in LB films [47]. The study of the molecule in the solvent used for the spreading process is necessary to verify that at the working concentration the Lambert –Beer law is followed (Equation 3.4) In this work, the spectra of the solutions were recorded using a quartz cell of 1 cm of path length.

$$A = \varepsilon . c . l \qquad (3.4)$$

where: ε is the molar absorption coefficient, c is the solute concentration and l is the path length.

This technique has also been used for the study of LB films deposited on quartz substrates [47]. These substrates are placed perpendicular to the UV-vis beam. The technique provides information on molecular interactions in the films (formation or absence of aggregates, etc..).

3.3.3. Cyclic voltammetry (CV)

The CV experiments were performed with an Autolab PGSTAT302N which is controlled by the specific program Autolab 4.9 software. Figure 3.9 shows images of this instrument, including the computer and the electrochemical cell with the electrodes.

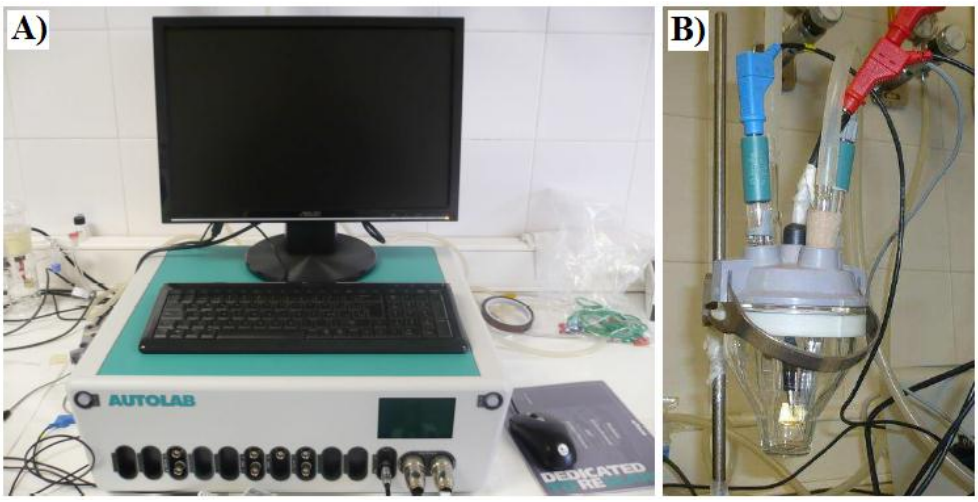

Figure 3.9. *A)* Autolab PGSTAT302N *and computer. B) Electrochemical cell with the electrodes [47].*

The cyclic voltammetry experiments were carried out using a three electrode (working, reference and auxiliary) system located within an electrochemical cell; the electrodes are in contact with a solution containing the electrolyte and the substance which acts as electrochemical redox probe. The working electrode is a LB film deposited on gold substrate from Arrandee®. The reference electrode was silver/silver chloride (Ag/AgCl (sat)), and the auxiliary electrode was a platinum foil.

Cyclic voltammetry is an electrochemical method that allows determining electrochemical properties of the films, and importantly it also provides an indirect measurement of holes or pores in the structure of the film by measuring the blocking of an underlying electrode when the LB film is transferred on its surface [60-63]. Cyclic voltammetry consists in producing a cyclic and linear variation of potential with the stationary working electrode (electrode in whose surface the electrochemical process under study takes place); the variation is in a potential range in which oxidation and reduction processes of the studied species occurs. In this process the variation of intensity versus potential is monitored and the resulting graph is called a voltammogram (Figure 3.10).

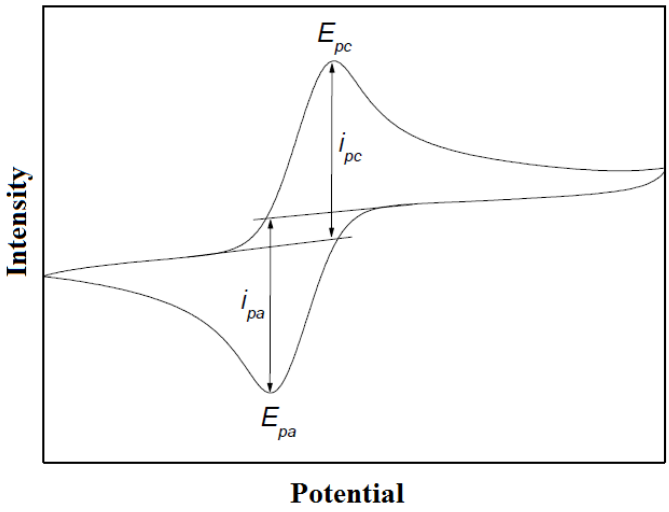

Figure 3.10. *Example of a voltammogram, where i_{pa}, E_{pa}, i_{pc} and E_{pc} are the maximum current density and the corresponding potential at the anodic and cathodic regions, respectively. The reverse cycle usually does not show the same behavior and amplitude as the forward sweep. It depends on the scan rate, reversibility of oxidation and reduction reactions, electrolyte concentration, surface roughness and the velocity of charge transfer into the electrolyte [47, 62].*

The instrumentation required for this technique is constituted by a potentiostate whose function is to control the potential applied to the working electrode with respect to the reference electrode and simultaneously to measure the current flow between the working electrode and auxiliary electrode. The device consists of a power supply that is located in a separate module. An electrochemical cell containing the electrolytic solution and the electrodes is connected to the potentiostate. The top of the cell has three holes to introduce the electrodes and it is also provided with an inlet and an outlet for the purge gas.

In the present work, the degree of blocking of the electrode surface modified by a LB film has been evaluated, which is an indirect way to detect the presence of holes or defects in the films [63]. The electrolytic solution used was an aqueous solution 0.1 M *KCl* and 1 mM of a salt which acts as a redox probe; this can be $K_3[Fe(CN)_6]$ or $[Ru(NH_3)_6]Cl_3$ depending on the composition of the LB film studied. *KCl* acts like a supporting electrolyte; it is responsible for ion transport and it serves to complete the circuit of the electrochemical cell. *KCl* functions are to provide a low electrical resistance,

maintaining a constant ionic strength of the medium and eliminating the effect of the current migration. This current migration is the result of the movement of ions and is caused by the electric field originated by the potential difference between the working electrode and the auxiliary electrode. In contrast, the role of redox probe is to provide information on the degree of blocking of the working electrode by the deposited monolayer.

3.3.4. Atomic force microscopy (AFM)

AFM experiments of LB and SA films were obtained with a Multimode 8 of the commercial Veeco belonging to the Laboratory of Advanced Microscopies (LMA). The characterization of the films was carried out in intermittent contact mode or "tapping" with a silicon tip from Bruker with a resonance frequency of 300 kHz and a constant force of 40 mN. Images were recorded with high resolution (512 lines/sample) at a scan rate of 1 Hz in air.

The AFM creates surface images of the films from the forces of attraction and repulsion between two bodies, the microscope tip and the sample under study. The system consists of a small probe tip which interacts with the sample surface; the tip is located at the end of a flexible sheet or cantilever. The tip scans the surface and it is moved vertically by atomic forces. These forces (attractive or repulsive) depend on the distance between the tip and the sample. A laser beam is focused in the tip and it is reflected to a photodetector, which transforms by means of the appropriate software this information into a surface image [64-65]. Operation of the AFM is shown in Figure 3.11.

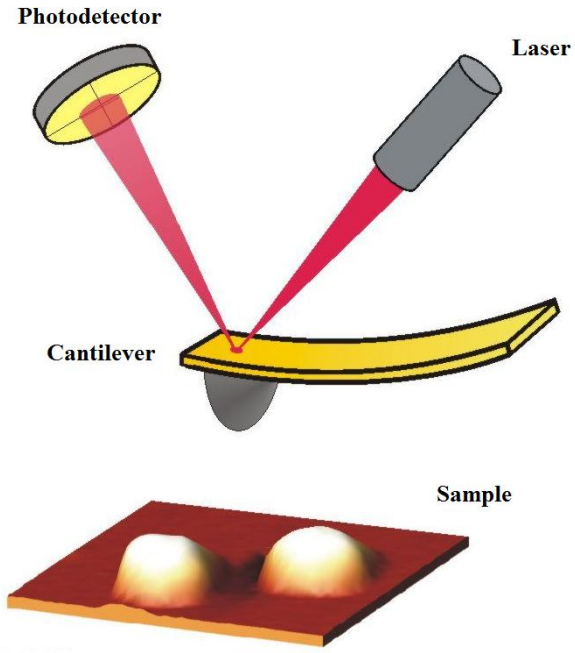

Figure 3.11. *AFM operation scheme [66].*

3.4. SINGLE MOLECULE CONDUCTANCE

Single molecule conductance measurements require certain guidelines and provisions in order to be sure about the observations realized. The following list deals with these issues in no particular order. To begin with, it is needed a recognizable signature to pick out the conductance of an individual molecule from an ensemble of molecules. A proper contact between both ends of the molecule with the electrodes (in a two terminal device) must be ensuring. Each measurement of a single molecule must be as similar to any other single molecule measurement to give reproducibility between experiments, hence making for reliable comparisons. Currently there are a few techniques which can fulfill all these criteria. They are scanning probe techniques based on STM, AFM, along with mechanically controlled break junctions [67] of the cantilever type.

In an STM or CAFM experiment the molecules of interest are firstly adsorbed onto the substrate. This is normally gold, due to its high affinity towards the thiol group, although other functional groups and substrates can be and are used. The molecular adlayer

can be relatively well defined; however, the tip-molecule-substrate arrangement is generally less well defined during an actual measurement, due to the variability in adsorption geometries on the tip (which generally has a non-crystalline structure). Essentially three STM based approaches have been developed.

3.4.1. STM-Break junction technique

The STM break junction method was introduced by N.J. Tao et al. [68] in 2003 and it involves the repeated mechanical contact between an STM tip and a metal substrate. The tip is first moved into mechanical contact with a covered surface (experiments are generally performed in a solution of the compound). Once contact has been established the tip is withdrawn, ultimately forming an atomic chain of metal atoms. When this chain cleaves a gap is left into which a molecule can bind, creating a metal-molecule-metal junction. During the initial stages of breaking tip contact with the substrate, the measured conductance decreases in a stepwise fashion, each step corresponding to an integer number of the conductance quantum $G_0 = 2e^2/h \approx 77.400$ μS. After the atomic chain has broken, by pulling further on the tip an extra sequence of steps at a lower conductance is apparent in the presence of molecules; a scheme of the process is shown in Figure 3.12. The conductance steps are due to the formation of stable molecular junctions, and a histogram analysis reveals the value of the lowest conductance value, associated to a single molecule junction.

3.4.2. *I(s)* technique [69]

The *I*(*s*) technique employs a similar experimental set-up as the break junction method, however, rather than making mechanical contact between the STM gold tip and the substrate, the tip is positioned at a defined distance from the surface whilst maintaining a constant *x*-*y* position. From this initial position, which is close enough for molecules to bridge the gap spontaneously, the tip is withdrawn until that the metal-molecule-metal bridge is broken. A scheme of the process is shown in Figure 3.13. This method was developed in Liverpool and it has been mainly used in this work.

Two distinctive classes of *I(s)* scans can be observed when performing the experiment. Curves with a fast exponential decay which is typical of tunneling between a tip and a bare metal that is, no molecular wire formation (curve 1 in Figure 3.14). The other curves show a less abrupt decay followed by a characteristic current plateau (I_w) associated to molecular wire formation (curve 2 in Figure 3.14).

The experiment is repeated many times, and the results are analyzed statistically. The data points in *I(s)* scans containing clear molecular plateaus are finally added together into one histogram, which gives peaks at the values characteristic of the average plateau positions in the measurements.

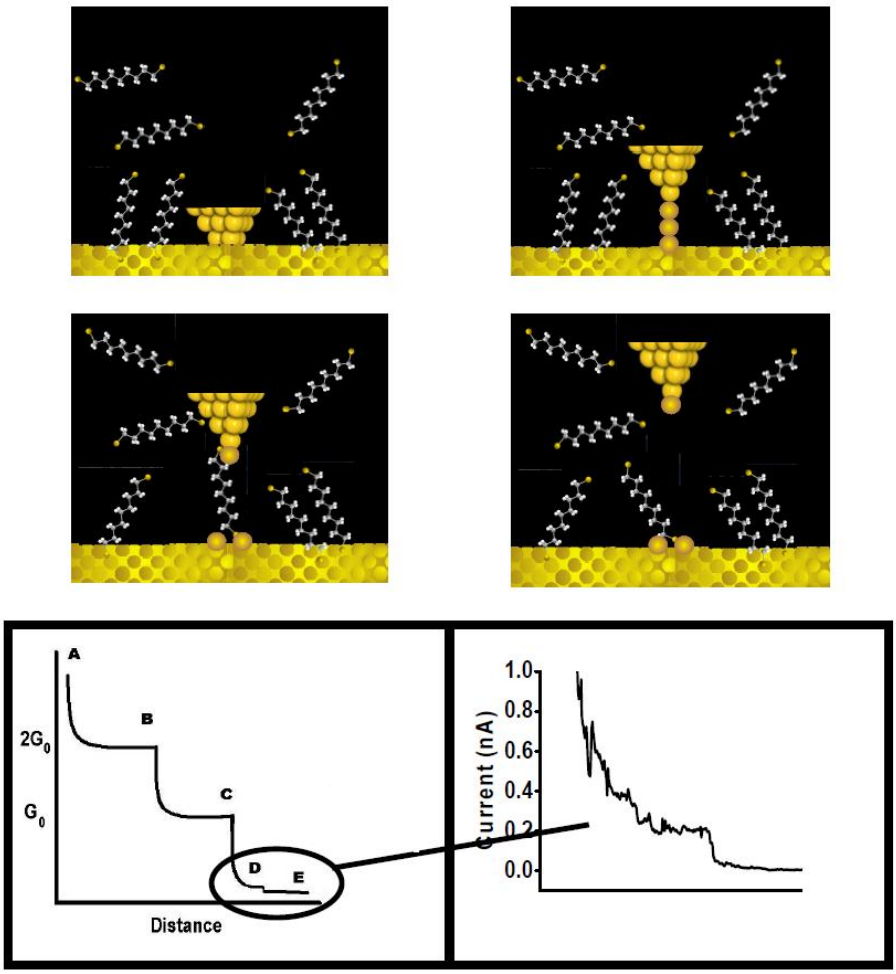

Figure 3.12. *An illustration of the steps in the break junction technique and the corresponding features in the current-distance trace.*

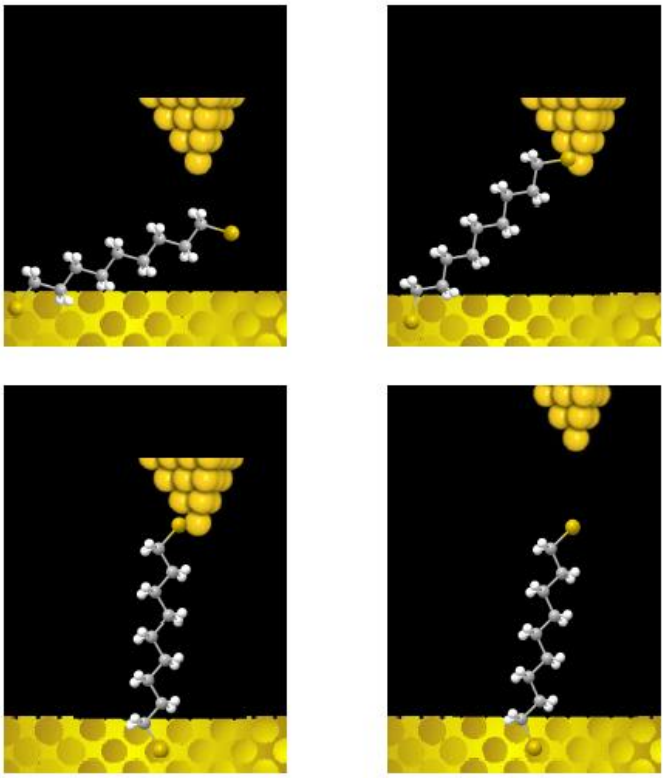

Figure 3.13. *An illustration of the different steps in an I(s) measurement.*

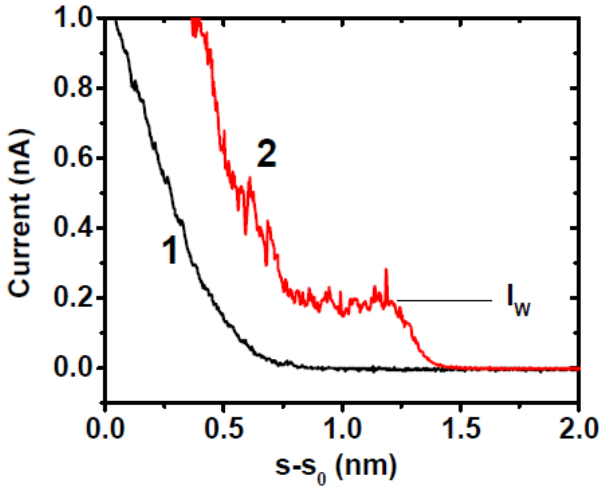

Figure 3.14. *Current decay curves in the I(s) technique. (1) No molecular wire formation. (2) Molecular wire formation associated to the plateau observed during the scan.*

4. STUDY AND CHARACTERIZATION OF LANGMUIR AND LANGMUIR-BLODGETT FILMS INCORPORATING AN ORGANOMETALLIC COMPOUND.

4.1. LANGMUIR FILMS

$trans - Ru(-C \equiv C - C_6H_4 - C \equiv C - SiMe_3 - 4)_2(dppe)_2$ in this work abbreviated as *TMS-Ru-TMS*, Figure 4.1 is an organometallic compound of high interest in molecular electronics, as it was mentioned in the introduction, due to the incorporation of ruthenium atom in the π-conjugated backbone and the use of trimethylsilane (TMS) like anchoring group between molecule and substrate.

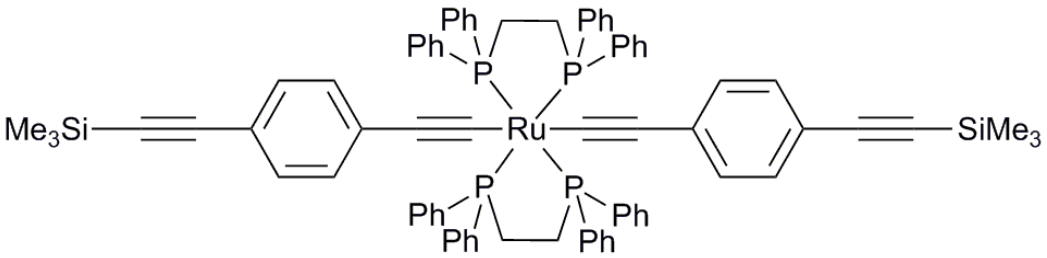

Figure 4.1. *TMS-Ru-TMS structure used in this work.*

UV-vis spectra of *TMS-Ru-TMS* in $CHCl_3$ at several concentrations were recorded and are shown in Figure 4.2. The spectra exhibit two absorption maximum at 276 nm and 382 nm. The Lamber-Beer law (Equation 3.4) is followed in the whole concentration range studied. From these data the molar absorptivity (ε) was calculated, with values of 48080 $L \cdot mol^{-1} \cdot cm^{-1}$ for the 276 nm band and 71390 $L \cdot mol^{-1} \cdot cm^{-1}$ for the 382 nm band.

After a preliminary study in which both the concentration and the volume of the spreading solution was varied, the optimum conditions for the preparation of the Langmuir films were a 10^{-5} M concentration of *TMS-Ru-TMS* in $CHCl_3$ and a volume of the spreading solution that yields an initial surface coverage of 4.78 $nm^2 \cdot molecule^{-1}$. In addition, the solution was sonicated for 10 minutes before the spreading process to minimize aggregation phenomena. Under these experimental conditions reproducible π-*A* isotherms were

obtained as illustrated in Figure 4.3. These isotherms were recorded at a compression speed of 0.018 $nm^2 \cdot molecule^{-1} \cdot min^{-1}$, a constant temperature of 20 ºC and using Milli-Pore Milli-Q water in the subphase (resistivity of 18.2 MΩ·cm).

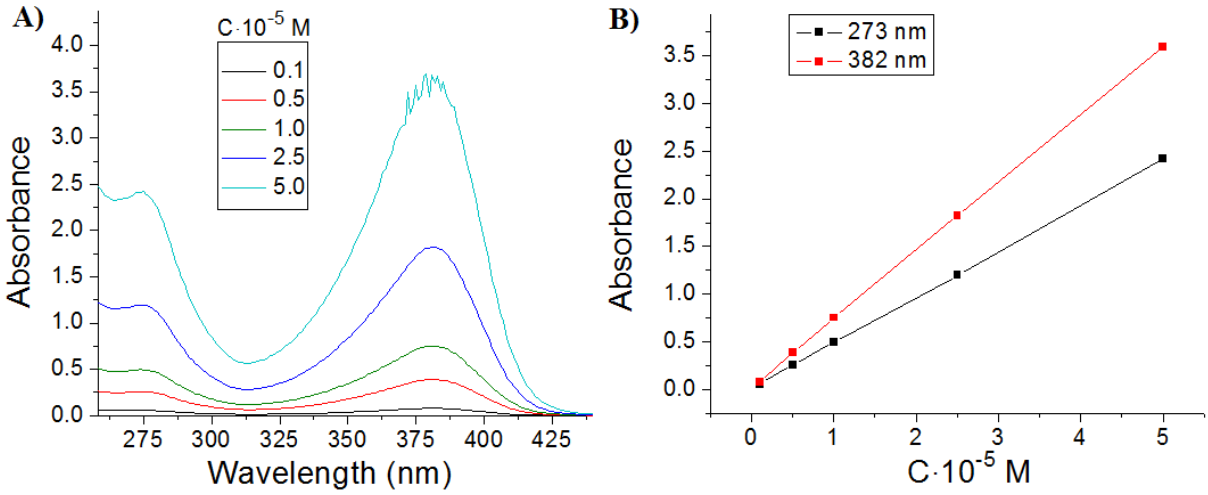

Figure 4.2. *Results of UV-vis spectroscopy of TMS-Ru-TMS. A) UV-vis spectra for different concentrations. B) Linear relationship between absorbance and concentration of the solution for 276 nm and 382 nm.*

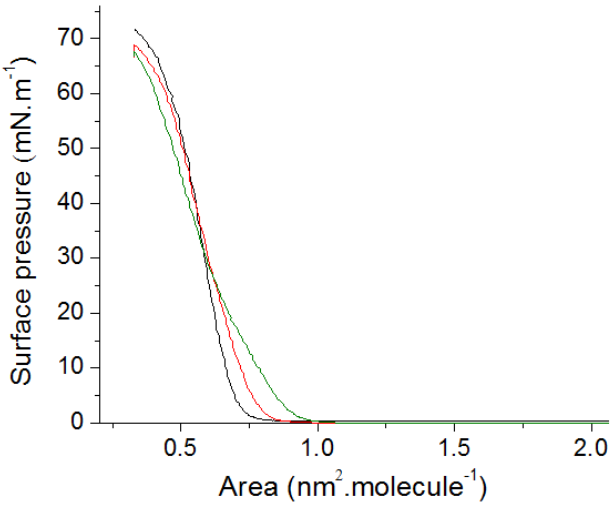

Figure 4.3. *Surface Pressure vs. Area per molecule isotherms of TMS-Ru-TMS recorded at 20 ºC.*

Surface potential vs. area per molecule (*ΔV-A*) isotherms were also recorded in order to obtain more details in the Langmuir film formation since *ΔV-A* isotherms provide

information of molecular reorganization processes occurring at the interface during the formation of films. In addition, *ΔV-A* isotherms allow the detection of changes in the organization of the molecules a few square Angstroms before changes can be detected by the *π-A* isotherm. The *ΔV-A* isotherm for *TMS-Ru-TMS* recorded at 20 ºC is shown in Figure 4.4.

Initially, a surface potential of 0 V is observed as expected for a non-ionized film. At an area of 3 $nm^2 \cdot molecule^{-1}$, the take-off in the surface potential isotherm takes place. This is indicative of a progressive orientation of the molecules even in the gas phase where $\pi \rightarrow 0$. The region between 3 and 1.2 $nm^2 \cdot molecule^{-1}$ is characterized by abrupt fluctuations in the surface potential values; these variations may be caused by the presence of small molecular aggregates or non-homogeneously distributed molecular domains in the gas phase. At areas lower than 1.2 $nm^2 \cdot molecule^{-1}$ a gradual increase in surface potential occurs until a value of 0.39 $nm^2 \cdot molecule^{-1}$ at which a decrease in the surface potential occurs. This sudden decrease in the surface potential value is consistent with a collapse of the monolayer, with dipole moments randomly distributed in a three dimensional arrangement of *TMS-Ru-TMS* molecules. It is noted at this point that transitions to a more condensed phase are characterised by an increase in ΔV values.

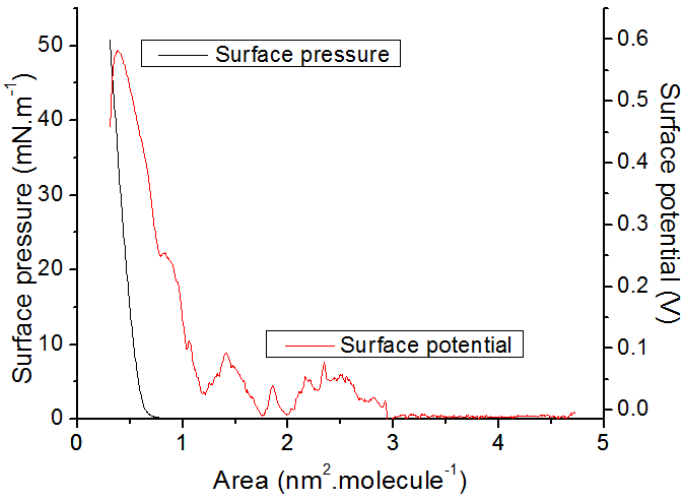

Figure 4.4. *Surface pressure and surface potential vs. area per molecule isotherms of TMS-Ru-TMS at 20 ºC.*

To corroborate these interpretations with some additional experimental data Brewster angle microscopy (BAM) images were recorded upon the compression of the monolayer. BAM images are shown in Figure 4.5. Bright white spots in Figure 4.5 A might indicate the presence of three dimensional aggregates or micro crystals. A decrease in the area per molecule results in a gradual covering of the water surface by the film. In addition, the images become brighter, indicating that the film thickness is increasing with decreasing area per molecule.

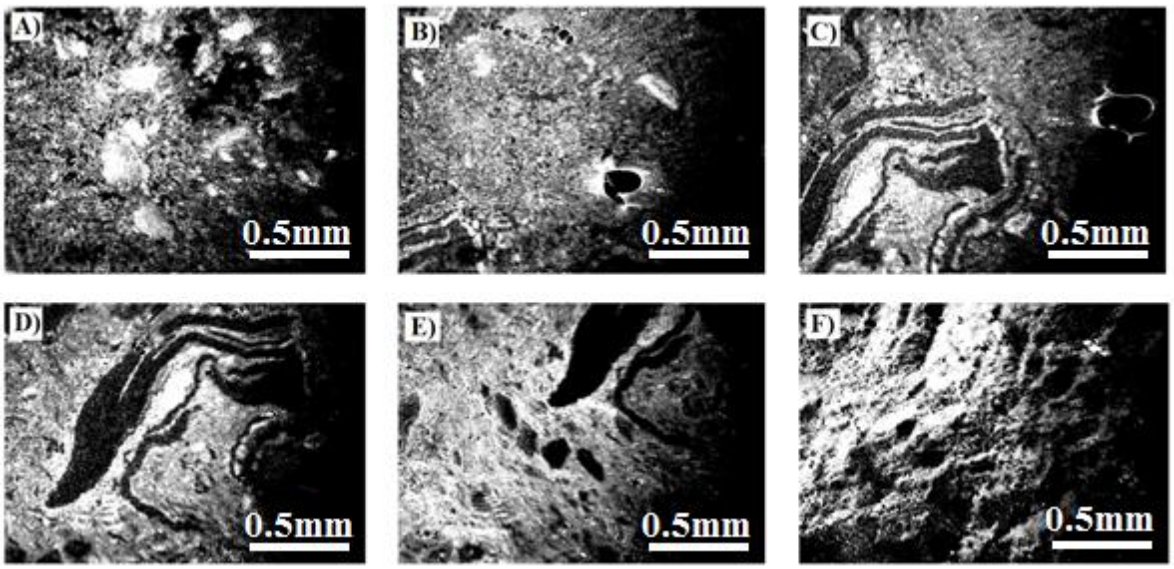

Figure 4.5. *BAM images at different conditions during the film formation of TMS-Ru-TMS. A)* $0\ mN.m^{-1}, 1.2nm^2.molecule^{-1}$, *B)* $5\ mN.m^{-1}, 0.92\ nm^2.molecule^{-1}$, *C)*$15\ mN.m^{-1}, 0.81\ nm^2.molecule^{-1}$, *D)* $25\ mN.m^{-1}, 0.69\ nm^2.molecule^{-1}$, *E)* $40\ mN.m^{-1}, 0.57\ nm^2.molecule^{-1}$, *F)* $60\ mN.m^{-1}, 0.47\ nm^2.molecule^{-1}$

4.2. LANGMUIR-BLODGETT FILMS

Langmuir films were transferred onto solid substrates. The films were deposited on different substrates, as required by the different characterization techniques. The transferences were made in the KSV Langmuir trough at a deposition speed of 5 mm·min^{-1}.

Firstly, one layer LB films were fabricated by emersion of mica substrates at different surface pressures of transference to determine the optimum surface pressure of

transference. The films were analyzed by atomic force microscopy (AFM). The AFM images are shown in Figure 4.6. These images show the presence of molecular aggregates as well as a non-well covered surface of the mica substrates.

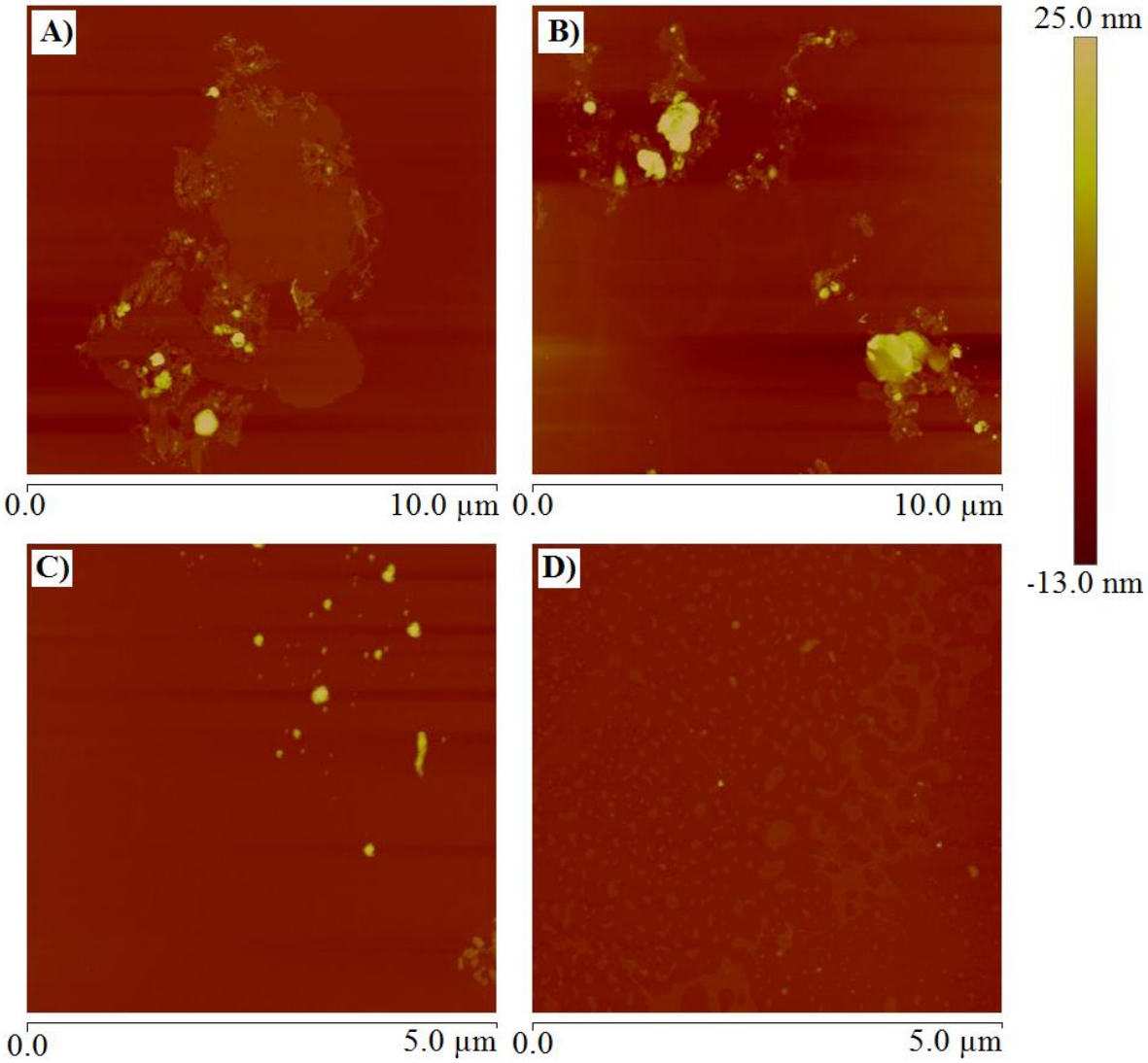

Figure 4.6. *AFM images at different surface pressures of transference of TMS-Ru-TMS. A)* 5 $mN.m^{-1}$, *B)* 10 $mN.m^{-1}$, *C)* 25 $mN.m^{-1}$, *D)* 40 $mN.m^{-1}$.

Then, transferences were made during the immersion of the substrate, with the AFM images of these films being shown in Figure 4.7. From these images it can be concluded that immersion of mica substrates leads to a better covering than films fabricated by the emersion of the substrates. However, the presence of aggregates is evident in both types of

films. Finally, these images reveal that a surface pressure of $25\ mN.m^{-1}$ yield the most homogeneous films.

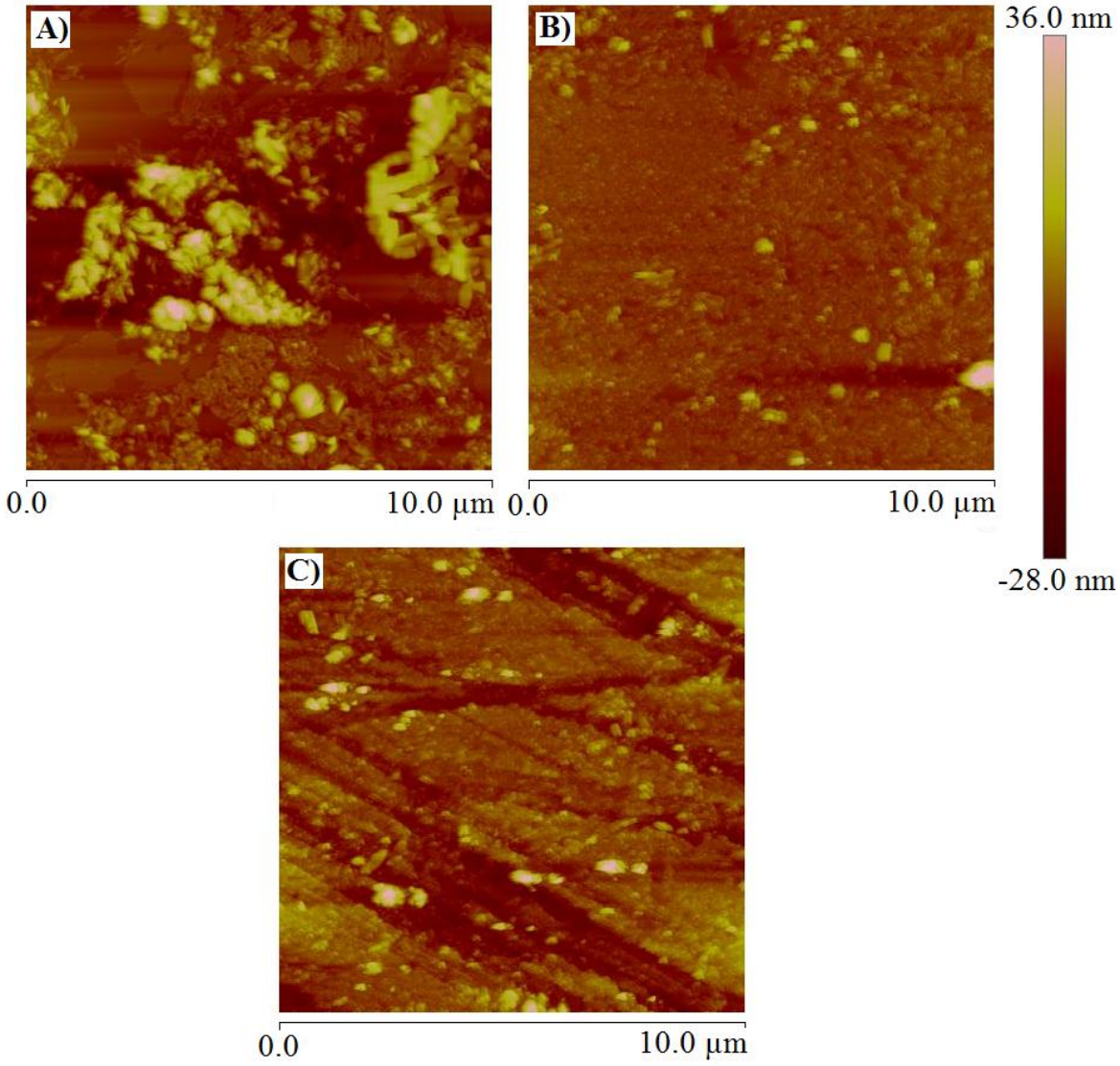

Figure 4.7. *AFM images at different surface pressures of transference of TMS-Ru-TMS films during the immersion of the mica substrate. A)* $10\ mN.m^{-1}$. *B)* $18\ mN.m^{-1}$. *C)* $25\ mN.m^{-1}$.

Cyclic voltammetry was used to evaluate the presence of holes in the transferred films. A monolayer of *TMS-Ru-TMS* was transferred onto a gold substrate that acts as the working electrode. The rest of the system is composed of a reference Ag/AgCl saturated electrode, a platinum electrode as a counter electrode and an aqueous solution formed by

$K_3[Fe(CN)_6]$ 1 mM (redox probe) and 0.1 M KCl (electrolyte). The scan speed was 0.05 $V \cdot s^{-1}$ and the potential was varied between 0.8 V and -0.2 V. The voltammograms of gold electrodes covered by one layer LB films transferred at 25 $mN.m^{-1}$ of surface pressure are shown in Figure 4.8.

The best blocking of the underlying gold electrode is obtained for substrates which are immersed in the subphase during the transference process, which indicates a better covering of the substrate with the film and lower amount of holes in the sample. These results are in good agreement with AFM images which revealed that films transferred during the emersion of the substrate present more defects (holes). Consequently, the results shown from bellow correspond to films transferred during the immersion of the substrate given that these films have a better quality.

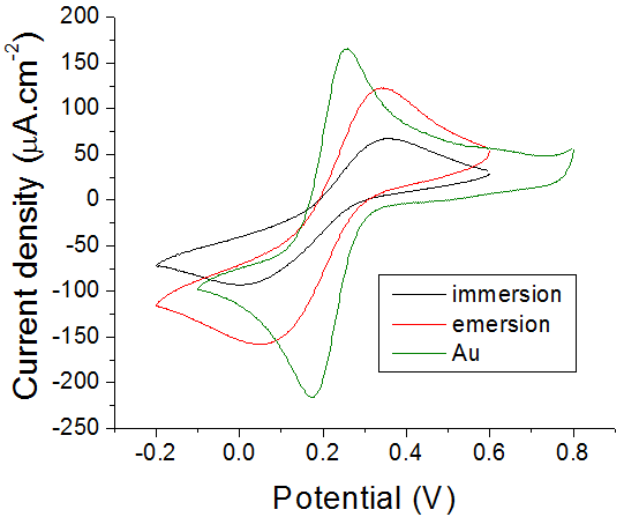

Figure 4.8. *Cyclic voltammetry of gold substrates covered by one layer LB films of TMS-Ru-TMS transferred during the immersion and the emersion of the gold substrate, also the voltammetry for gold without covering is showed for comparing.*

QCM was used to determine the surface coverage and transfer ratio of *TMS-Ru-TMS* films transferred during the immersion of the substrates at a surface pressure of 25 $mN.m^{-1}$. The QCM analysis showed a frequency variation of -61 Hz (substrate before and after the film deposition). Application of the Sauerbrey equation (Equation 3.2), the

surface coverage (that corresponds to the mass variation) was determined to be 4.17×10^{-10} mol. cm^{-2}.

The transference (τ) is defined as the relationship between the surface coverage of the monolayer at the air-water interface and the surface coverage in the substrate [70] as stated in Equation 4.1.

$$\tau = \frac{S_{air-water}}{S_{substrate}} \quad (4.1)$$

where $S_{air-water}$ is the surface coverage at the air-water interface (Langmuir film) and $S_{substrate}$ is the surface coverage of the substrate after the transference (LB film). Consequently, by applying Equation 4.1 a transfer ratio of 1.23 is obtained.

A single layer films incorporating *TMS-Ru-TMS* was transferred onto a quartz substrate and its UV-vis spectrum was recorded (Figure 4.9). The spectrum presents the same maximum absorption bands and a similar profile to that of the initial solution. This result indicates that no chemical reaction or degradation of the material has taken place during the assembling process.

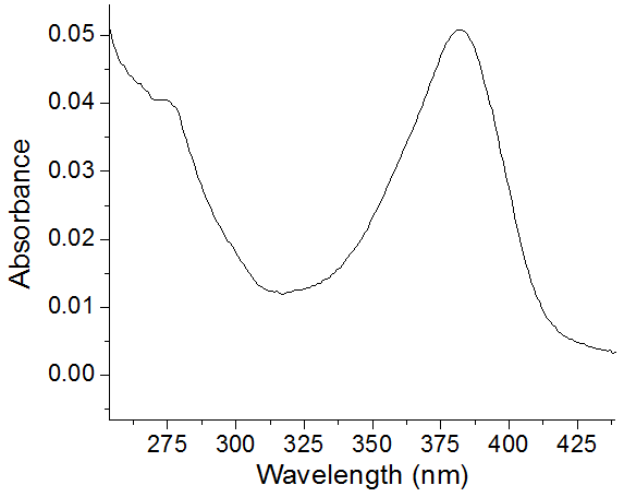

Figure 4.9. *UV-vis spectroscopy of quartz substrates covering incorporating TMS-Ru-TMS.*

The characterization of LB films incorporating *TMS-Ru-TMS* has revealed that these films do not perfectly cover the underlying substrate and present a significant number of

holes, defects, etc. compared with other films in the same family [71-73]. The main reason is the fact that *TMS-Ru-TMS* is a very hydrophobic material not easy to be assembled by the LB method. This is the reason why we have tried to improve the quality of the films by using alternative methods, as presented in the next section, i.e., the fabrication of a mixed film of *TMS-Ru-TMS* with an amphiphilic material capable of forming good LB films. The fabrication of mixed Langmuir films is well-known process which may result helpful in the assembly of non-amphiphilic materials into LB films [44, 74-75]

4.3. MIXED LANGMUIR FILMS OF *TMS-Ru-TMS* AND *TMS-OPE-NH₃Cl*

Chloride, 4 - (4 - (4 - (trimethylsilyl ethynyl) phenylethynyl) phenylethynyl)-benzenamine (abbreviated as *TMS-OPE-NH₃Cl*, Figure 4.10) is the material with which *TMS-Ru-TMS* has been mixed. This molecule was selected because it has a similar structure to *TMS-Ru-TMS* and because it is known that forms high quality LB films [43].

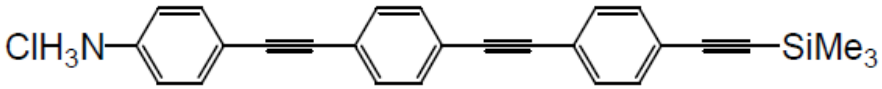

Figure 4.10. *TMS-OPE-NH₃Cl structure.*

Both *TMS-Ru-TMS* and *TMS-OPE-NH₃Cl* are soluble in chloroform and taken into account that this is a good solvent to be employed in the LB technique; solutions of these compounds were prepared in chloroform and were sonicated for 10 minutes to minimize molecular aggregation. Films of *TMS-OPE-NH₃Cl* were studied by Dr. Gorka Pera [43, 47]. This author demonstrated that 1.10^{-5} M solutions of *TMS-OPE-NH₃Cl* in chloroform follow the Lambert-Beer law and yield good L and LB films. These are the reasons why this concentration, in both compounds, was chosen to prepare the films. In particular, 3 mL of mixed solution were spread. Extra details in the Langmuir film construction are: compression speed of 0,018 $nm^2 \cdot molecule^{-1} \cdot min^{-1}$, working temperature of 20 ± 1 ºC and the subphase was Millipore Milli-Q water (resistivity of 18.2 MΩ·cm). *π-A* isotherms are shown in Figure 4.11.

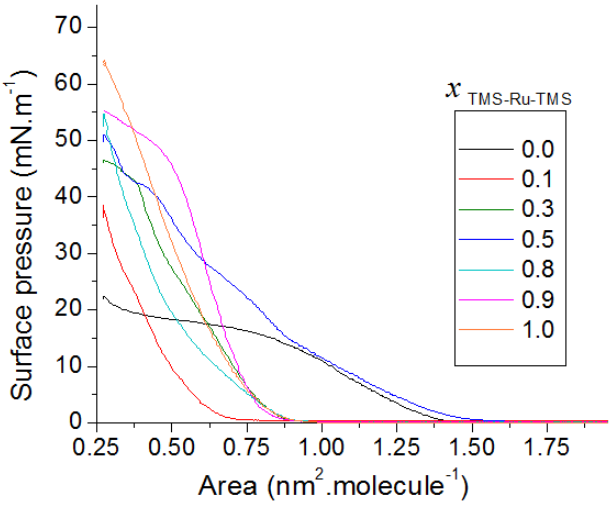

Figure 4.11. *π-A isotherms of the pure and mixed films recorded for the indicated TMS-Ru-TMS mole fraction.*

The nature of molecular interactions and also the miscibility of the two components can be examined by quantitative analysis of the excess area (A^E) of the mixed monolayer at the air–water interface. The excess area can be obtained by comparing the average area per molecule (A_{12}) of a mixed monolayer consisting of components 1 and 2 with that of an ideal mixed monolayer (A_{id}). The excess area is defined in equation 4.2 [44, 74-75].

$$A^E = A_{12} - A_{id} = A_{12} - (x_1 A_1 + x_2 A_2) \qquad (4.2)$$

where A_{12} is the experimental area per molecule in the mixed film at a given surface pressure, A_1 and A_2 are the areas per molecule at that surface pressure for the pure films, and x_1 and x_2 are their mole fractions. Figure 4.12 shows the excess area per molecule vs. the *TMS-Ru-TMS* mole fraction.

The excess Gibbs energy of mixing (ΔG_m^E), provides another indication of the interactions between components in mixed monolayers with reference to the interactions between molecules of the same kind before mixing, although entropic factors also contribute to the ΔG_m^E values. ΔG_m^E can be calculated by means of Equation 4.3 [44, 74-75].

$$\Delta G_m^E = \int_0^\pi A_{12}\, d\pi - x_1 \int_0^\pi A_1\, d\pi - x_2 \int_0^\pi A_2\, d\pi \qquad (4.3)$$

where A_{12}, A_1, A_2, $x_1$and x_2 have the same meaning as before; π is the upper limit pressure at which the integrals have been calculated. The results of ΔG_m^E for the system here studied are shown in Figure 4.13.

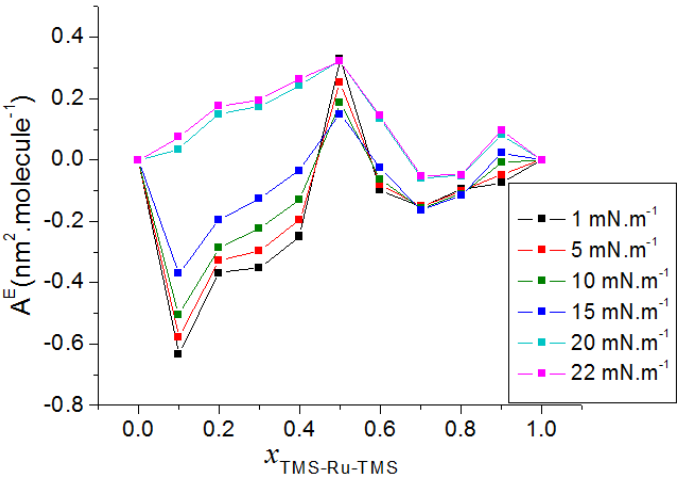

Figure 4.12. *Excess area vs. mole fraction of TMS-Ru-TMS for the indicated surface pressures.*

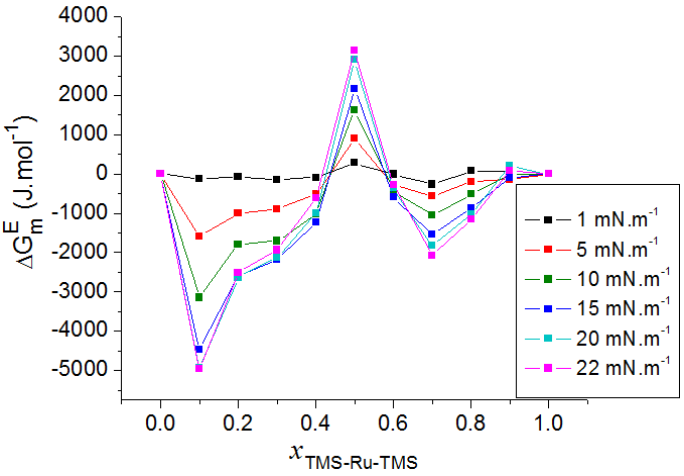

Figure 4.13. *Excess Gibbs energy of mixing vs. mole fraction of TMS-Ru-TMS for the indicated surface pressures.*

To ensure the reproducibility of the obtained results, the *π-A* isotherms and the thermodynamic analysis were repeated. The results are shown in Figure 4.14.

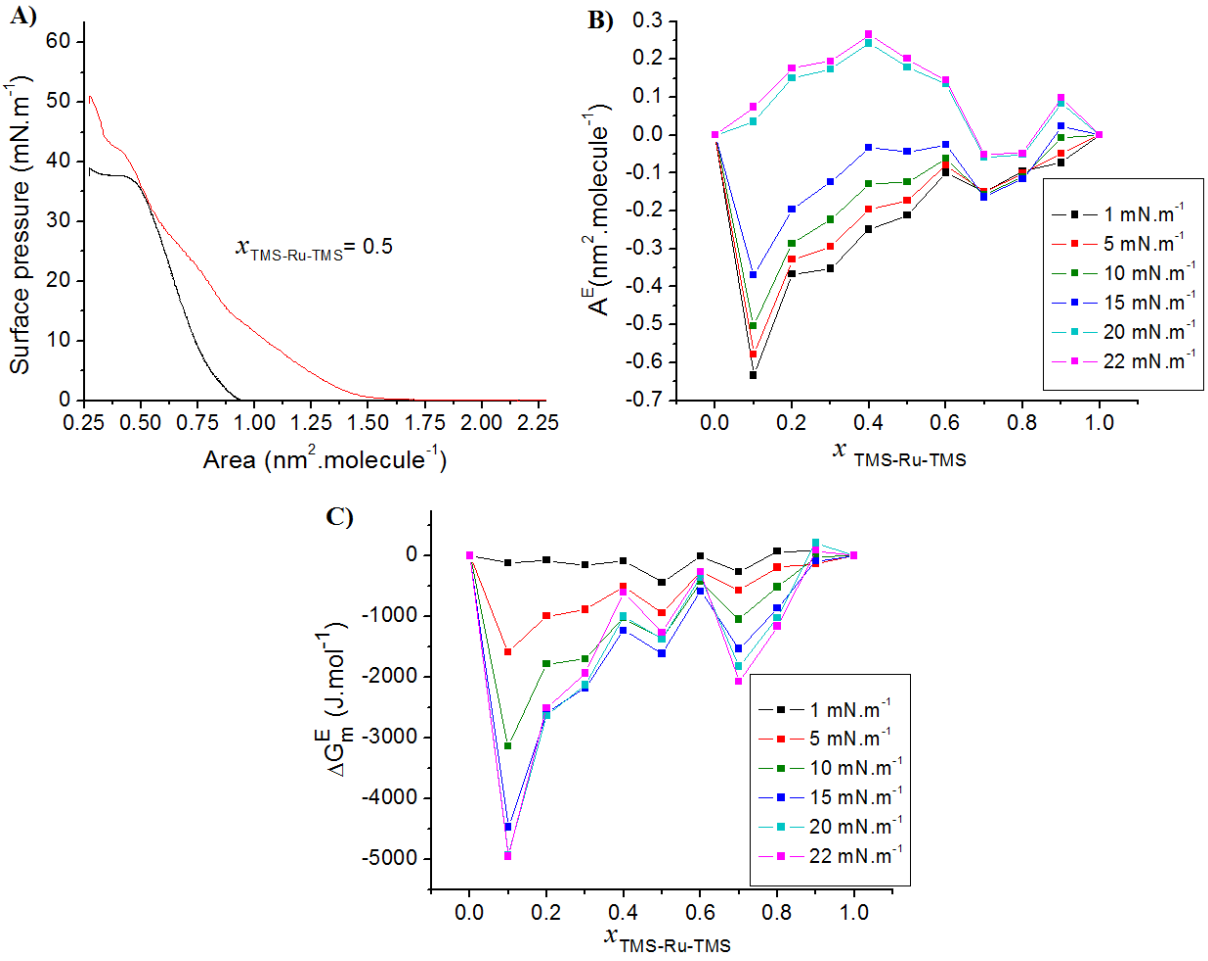

Figure 4.14. *Repetition in the analysis procedure of TMS-Ru-TMS/TMS-OPE-NH_3Cl system. A) π-A isotherms obtained at same condition than those in Figure 4.11. B) Excess area vs. mole fraction of TMS-Ru-TMS for the indicated surface pressures, C) Excess Gibbs energy of mixing vs. mole fraction of TMS-Ru-TMS for the indicated surface pressure.*

Figure 4.14 shows that the *π-A* isotherms are not reproducible specially in the proportion 1:1, this suggest that is complicated to obtain a good Langmuir film of *TMS-Ru-TMS* or any mixture at the air-water interface. For these reasons other deposition technique was explored, the self-assembly method.

4.4. SELF-ASSEMBLY FILMS

In the present work three molecules have been assembled by the SA method, Bis(dppe)-bis(ethynyl) Ruthenium (II) complex (abbreviated as *TMS-Ru-TMS*), 1, 4-bis((4-((trimethylsilyl)ethynyl)phenyl)ethynyl)benzene (abbreviated as *TMS-OPE-TMS*) and 1,4-bis(4-ethynylphenyl)ethynyl)benzene (abbreviated as *HC2-OPE-C2H*) whose molecular structures are shown in Figure 4.15. Solutions (1.10^{-5}M) of these materials were prepared in chloroform and sonicated for 10 minutes to minimize molecular aggregation. Gold substrates (Arrandee®, Schroeer, Germany) were used; they were heated with a Bunsen burner in order to obtain atomically flat Au(111) terraces [55].

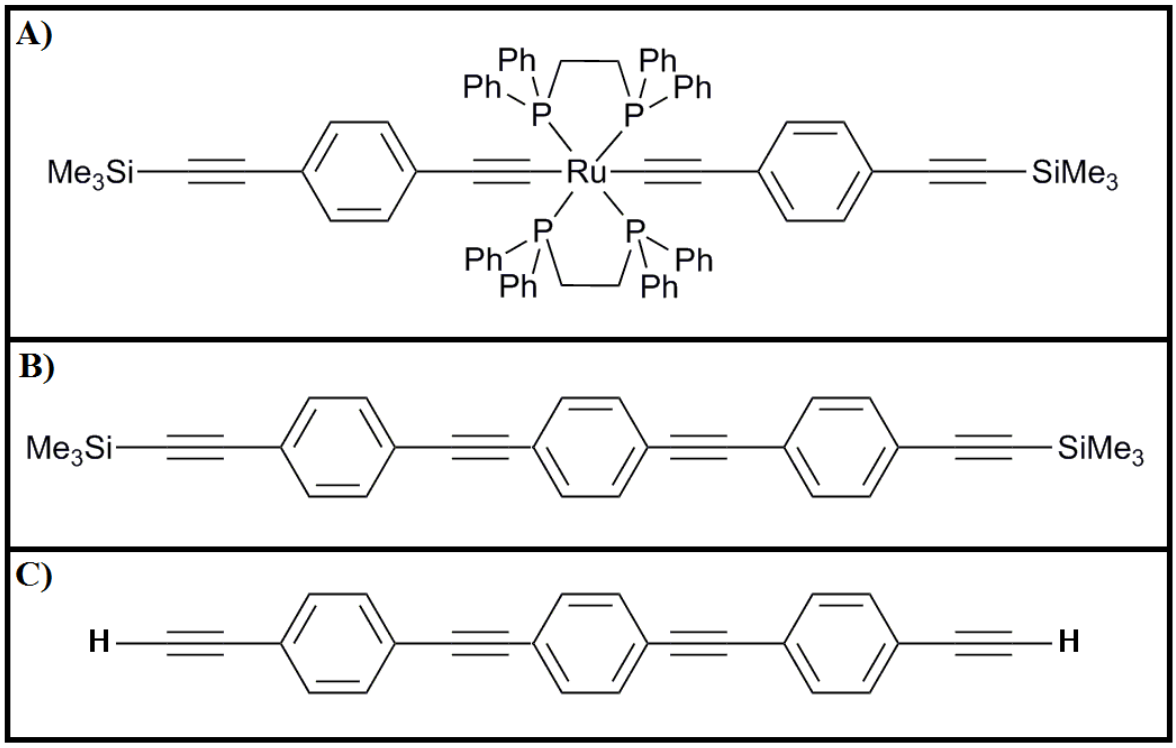

Figure 4.15. *Structures of molecules assembled by the SA method in this work. A) TMS-Ru-TMS. B) TMS-OPE-TMS. C) HC2-OPE-C2H.*

Molecules were prepared in a chloroform solution with concentration of 1×10^{-5} M, and substrates were immersed 4 days for their incubation to ensure the complete covering, finally all processes and measures were made at 20 °C. The surface coverage of gold

substrates after incubation in the organic solutions as explained above was studied with the QCM. The results are gathered in Table 4.1.

Table 4.1. *Variation in the QCM frequency before and after deposition of the indicated material by the SA method and surface coverage calculated according to the Sauerbrey equation.*

Molecule	**Δf QCM (Hz)**	**Γ (mol. cm^{-2})**
TMS-Ru-TMS	- 57	3.90×10^{-10}
TMS-OPE-TMS	- 39	7.20×10^{-10}
HC2-OPE-C2H	- 30	8.12×10^{-10}

Comparing the results for *TMS-Ru-TMS* between LB and SA films, a higher deposition is obtained with LB technique. This result is due to that LB films are formed by multilayer and/or aggregates of molecules, while SA films are formed by monolayers; without aggregates.

The morphology of the SA films was studied with AFM. Figure 4.16 shows the images of these monomolecular LB films where a high degree of order and homogeneity is observed. In addition, the roughness of the films is 1.50, 2.00, and 2.50 nm, respectively. Thus, we can say that films of this compound can be prepared using the self-assembly method.

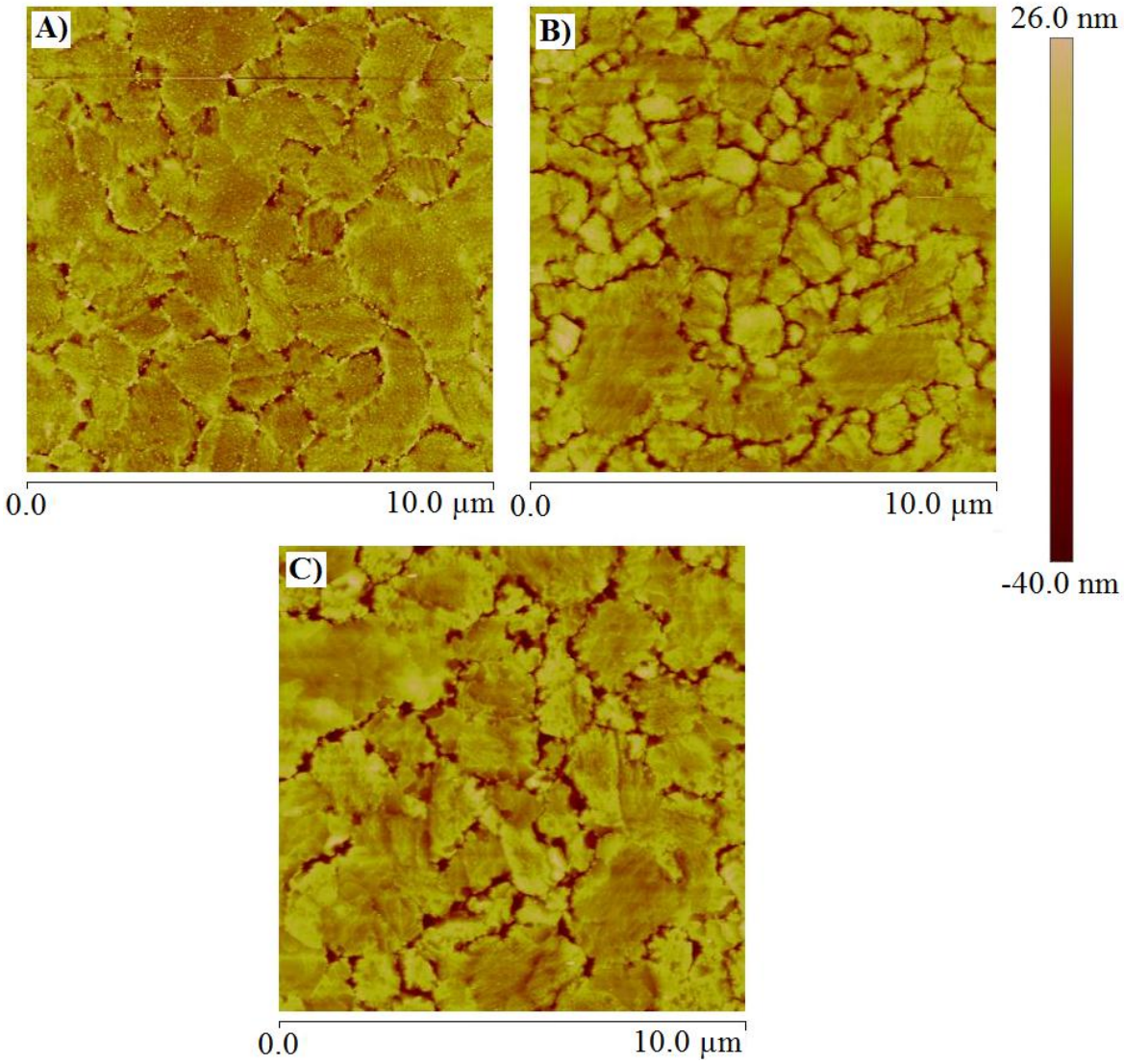

Figure 4.16. *AFM images of Self-assembly study. A) TMS-Ru-TMS, B) TMS-OPE-TMS, C)HC2-OPE-C2H*

4.5. SINGLE MOLECULE CONDUCTANCE FOR *TMS-Ru-TMS* AND *TMS-OPE-TMS*

To carry out the single molecule conductance gold substrates (Arrandee®, Schroeer, Germany) were used which were previously heated with a Bunsen burner in order to obtain atomically flat Au(111) terraces [55]. Both molecules were then adsorbed by immersion of the substrate in solutions 1×10^{-5} M in THF of these compounds for about 30 seconds.

The low concentration and relatively short immersion times are required in order to promote low surface coverage on the gold substrate, consequently single molecule are adsorbed. After adsorption, the sample was washed in ethanol and then blown dry in a stream of nitrogen gas to eliminate the molecules which are not chemisorbed. As a STM tip, a gold wire was used which was freshly prepared for each experiment by etching of a 0.25 mm Au wire (99.99%) in a mixture of HCl (50%) and ethanol (50%) at 2.4 V [55].

The results of single molecule measures using *I(s)* technique are shown in Figure 4.17. Figure 4.17A and 4.17B are presented with the tunneling conductance on the *y*-axis and distance displacement on the *x*-axis (distance displacement from the set-point distance from which the tip is retracted following disengagement of the feedback loop). These curves exhibit current steps which are attributed to the breaking of molecular bridges that were attached between tip and sample at the start of the tip retraction scan. Conductance histograms show single conductance values of $5.10 \pm 0.99 \times 10^{-5}\ G_o$ (*TMS-Ru-TMS*) and $2.75 \pm 0.56 \times 10^{-5}\ G_0$ (*TMS-OPE-TMS*). Measures were taken at different randomly selected locations of the sample.

Comparing results of conductance values $5.10 \pm 0.99 \times 10^{-5}\ G_0$ and $2.75 \pm 0.56 \times 10^{-5}\ G_0$ of *TMS-Ru-TMS* and *TMS-OPE-TMS*, respectively, the higher conductivity of the organometallic molecular junction from *TMS-Ru-TMS* is consistent with the slightly shorter length of the molecule, and the better alignment of the molecular HOMO with the Fermi levels of the gold contacts. In addition, the structure of backbone plays an important role in molecular conductance for *TMS-Ru-TMS*. The ruthenium-acetylene bond has high electron mobility delocalizing the backbone [76]; this experimental observation is according with the results reported by Liu et al. [38].

The single molecule conductance values obtained in this study are in the same order to these obtained by Lu et al. [77] using the BJ method and similar compounds, in his study the $-\mathrm{C} \equiv \mathrm{CSiMe_3}$ terminal groups were changing by $-\mathrm{NH_2}$. This result indicates that both groups have similar electrical characteristics contacts and that trimethylsilylethynyl is an alternative anchoring group providing effective electronic coupling at metal-molecule contacts.

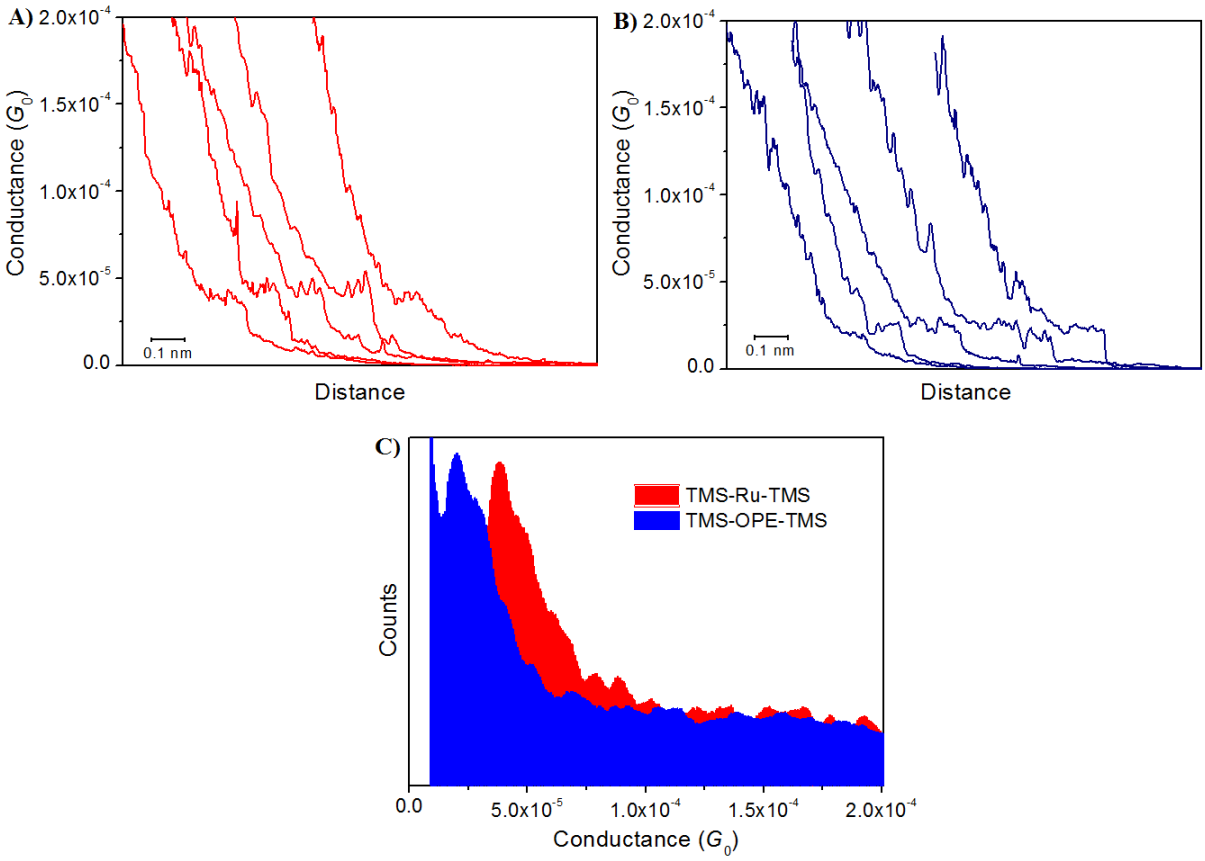

Figure 4.17. *Conductance traces recorded using the I(s) technique for (A) TMS-Ru-TMS and (B) TMS-OPE-TMS, curves are shifted horizontally for clarity, and (C) conductance histograms built by adding together all the points of conductance traces that showed discernible plateaus. Conductance data are presented in units of the conductance quantum* $G_0 = 2e^2/h = 77.5\,\mu S.\ U_t = 0.6\,V.$

Finally, an important characteristic observed along the single molecule conductance measurements for these compounds is that only an unique value of conductance has been measured using the I(s) technique. Comparing this result with the reported in the literature [77] for similar molecules with other terminal groups, these compounds showed three conductance values. In the present study the only conductance value obtained is located in the "low conductance" regime meanwhile others conductance values located in the "medium and high conductance" regime were not observed. This result corroborates the idea that the additional steric bulk of the $SiMe_3$ group limit the range of accessible surface binding sites overall to the higher coordinate defect sites.

CONCLUSIONS

The objective proposed at the beginning of this work was to fabricate metal/organic monolayer/metal devices, incorporating materials with potential applications in molecular electronic. The studied molecules were oligo(phenylene)ethynylene derivatives (OPEs). Firstly, the possibility to assemble an organometallic compound onto thin films by the Langmuir-Blodgett (LB) technique was studied. After, the use of Self-Assembly (SA) method was analyzed due to the LB technique yielded a non-homogenous film with the presence of aggregates. The prepared films were characterized by using a wide range of optical, spectroscopic and scanning probe techniques to determine the molecular arrangement of the material in the film. Finally, the study of single molecule conductance was carried out in order to know important characteristics of the TMS group like anchorage group in metal-molecule-metal junctions.

The *TMS-Ru-TMS* compound has the requirements to be transferred by Langmuir-Blodgett technique on a substrate. Thus, the molecule has a polar group to benefit the anchoring of the molecule onto the water subphase and a hydrophobic part to stabilize the films at the air-water interface. Nevertheless, this work shows that these characteristics are not enough to obtain good Langmuir films at the air-water interface due probably to the nonlinearity in the hydrophobic part caused for the atoms located around of the ruthenium atom. Therefore, the possibility of preparing LB films of *TMS-Ru-TMS* and its mixture with *TMS-OPE-*NH_3Cl, which forms stable and homogenous Langmuir films was analyzed. In this later case, the isotherms were not reproducible so, this suggests that is complicated to obtain a good Langmuir film of *TMS-Ru-TMS* or any mixture at the air-water interface.

Self-assembly method was employed in order to obtain good monolayers of this compound, *TMS-Ru-TMS*; with this technique a good covering was obtained. These good results are thanks to the TMS group, specifically by the silicon atom that is chemisorbed in the gold surface for *TMS-Ru-TMS* and *TMS-OPE-TMS*, and also a good chemisorption is showed for *HC2-OPE-C2H* thanks to the HC_2 terminal group.

Single molecule conductance measurements were made in order to know the electrical characteristics of *TMS-Ru-TMS* and *TMS-OPE-TMS* and their possible use in

molecular electronic. This study shows important results. Firstly, the conductance value obtained for the *TMS-OPE-TMS* is similar to other compounds studied but with different anchorage groups. Secondly, thanks to the TMS group these molecules present only a unique conductance value. Finally, the incorporation of ruthenium complex into the backbone of molecule increases the conductance value. Therefore, we could conclude that: TMS group may be a potential anchorage group in molecular electronics and also that the incorporation of ruthenium may be a potential choice for constructing long molecular wires with high conductance. Then we propose the use of *TMS-Ru-TMS* as a molecular wire with high conductance in molecular electronic.

REFERENCES

[1] C. Kergueris, J. P. Bourgoin, S. Palacin, D. Esteve, C. Urbina, M. Magoga, and C. Joachim. *Phys. Rev. B*. **1999**, *59*, 12505.

[2] S. Lenfant, D. Guerin, F. Tran Van, C. Chevrot, S. Palacin, J. P. Bourgoin, O. Bouloussa. F. Rondelez, and D. Vuillaume. *J. Phys. Chem. B*. **2006**, *110*, 13947.

[3] D. I. Son, T. W. Kim, J. H. Shim, J. H. Jung, D. U. Lee, J. M. Lee, W. I. Park, and W. K. Choi. *Nano Lett.* **2010**, *10*, 2441.

[4] R. J. Tseng, J. Huang, J. Ouyang, R. B. Kaner, and Y. Yang. *Nano Lett*. **2005**, *5*, 1077.

[5] D. I. Son, J. H. Kim, D. H. Park, W. K. Choi, F. Li, J.H. Ham, and T. W. Kim. *Nanotechnology*. **2008**, *19*, 055204.

[6] S. Tatay. *Complejos metálicos biestables para la electrónica molecular: síntesis y organización sobre superficies de rotaxanos y moléculas imán*. Dissertation to obtain the degree of Doctor: Universidad de Valencia, Valencia-Spain, **2008**.

[7] H. Kahuakami, H. Kato, and K. Yamashiro. *Fuji Electric Review*. **2005**, *50*, 72.

[8] Q. Chen, H. Bai, and G. Q. Shi. *Chinese Science Bulletin*. **2007**, *52*, 2017.

[9] L. P. Ma, J. Liu, and Y. Yang. *Appl Phys Lett*. **2002**, *80*, 2997.

[10] D. I. Son, C. H. You, W. T. Kim, J. H. Jung, and T. W. Kim. *Appl Phys Lett*. **2009**, *94*, 132103.

[11] D. I. Son, T. W. Kim, J. H. Shim, J. H. Jung, D. U. Lee, J. M. Lee, W. I. Park, and W. K. Choi. *Nano Lett*. **2010**, *10***,** 2441.

[12] J. G. Park, G. S. Lee, K. S. Chae, Y. J. Kim, and T. Miyata. *Korean Phys. Soc*. **2006**, *48*, 1505.

[13] T. Nakamura, S. Yasuda, T. Miyamae, H. Nozoye, N. Kobayashi, H. Kondoh, I. Nakai, T. Ohta, D. Yoshimura, and M. Matsumoto. *J. Am. Chem. Soc*. **2002**, *124*, 12643.

[14] R. J. Tseng, J. Huang, J. Ouyang, R. B. Kaner, and Y. Yang. *Nano Lett*. **2005**, *5*, 1077.

[15] M. Cölle, B. M, de Leeuw D M. *Organ Electron.* **2006**, *7*, 305.

[16] A. Nitzan, and M. A. Ratner. *Science.* **2003**, *300*, 1384.

[17] W. Chen, L. Wang, C. Huang, T. T. Lin, X. Y. Gao, K. P. Loh, Z. K. Chen, and A. T. Shen-Wee. *J. Am. Chem. Soc*. **2006**, *128*, 935.

[18] M. Kiguchi, S. Miura, K. Hara, M. Sawamura, and K. Murakoshi. *Appl. Phys. Lett*. **2006**, *89*, 213104.

[19] K. Yokota, M. Taniguchi, H. Tanaka, and T. Kawai. *Phys. Rev. B.* **2008**, *77*, 165416.

[20] G. Heimel, L. Romaner, E. Zojer, and J. L. Brédas. *Nano Lett*. **2007**, *7*, 932.

[21] G. Heimel, L. Romaner, J. L. Brédas, and E. Zojer. *Phys. Rev. Lett*. **2006**, *96*. 196806.

[22] F. Rissner, Z. Y. Ma, O. T. Hofmann, C. Slugovc, Z. Shuaie, and E. Zojer. *J. Mater. Chem*. **2012**, *22*, 4269.

[23] G. Heimel, L. Romaner, J. L. Brédas, and E. Zojer. *Surf. Sci*. **2006,** *600*, 4548.

[24] L. A. Zotti, T. Kirchner, J. C. Cuevas, F. Pauly, T. Huhn, E. Scheer, and A. Erbe. *Small*. **2010**, *6*, 1529.

[25] J. M. Seminario, C. E. De La Cruz, and P. A. Derosa. *J. Am. Chem. Soc*. **2001**, *123*, 5616.

[26] D. L. DuBose, R. E. Robinson, T. C. Holovics, D. R. Moody, E. C. Weintrob, C. L. Berrie, and M. V. Barybin. *Langmuir.* **2006**, *22*, 4599.

[27] K. Yokota, M. Taniguchi, and T. Kawai. *J. Am. Chem. Soc*. **2007**, *129*, 5818.

[28] A. Shaporenko, P. Cyganik, M. Buck, A. Terfort, and M. Zharnikov. *J. Phys. Chem. B*. **2005**, *109*, 13630.

[29] X. S. Zhou, Z. B. Chen, S. H. Liu, S. Jin, L. Liu, H. M. Zhang, Z. X. Xie, Y. B. Jiang, and B. W. Mao. *J. Phys. Chem. C.* **2008**, *112*, 3935.

[30] M. Kamenetska, M. Koentopp, A. C. Whalley, Y. S. Park, M. L. Steigerwald, C. Nuckolls, M. S. Hybertsen, and L. Venkataraman. *Phys. Rev. Lett*. **2009**, *102*, 126803.

[31] C. Wang, A. S. Batsanov, M. R. Bryce, S. Martín, R. J. Nichols, S. J. Higgins, V. M. Garcia, and C. J. Lambert. *J. Am. Chem. Soc*. **2009**, *131*, 15647.

[32] S. Y. Quek, M. Kamenetska, M. L. Steigerwald, H. J. Choi, S. G. Louie, M. S. Hybertsen, J. B. Neaton, and L. Venkataraman. *N. Nano. Lett*. **2009**, *4*, 230.

[33] M. Kamenetska, S. Y. Quek, A. C. Whalley, M. L. Steigerwald, H. J. Choi, S. G. Louie, C. Nuckolls, M. S. Hybertsen, J. B. Neaton, and L. Venkataraman. *J. Am. Chem. Soc*. **2010**, *132*, 6817.

[34] S. V. Aradhya1, M. Frei1, M. S. Hybertsen, and L. Venkataraman. *N. Mat. Lett*. **2012**, *10*, 1038.

[35] K. Heister, H.T. Rong, M. Buck, M. Zharnikov, M. Grunze, and L. S. O. Johansson. *J. Phys. Chem. B.* **2001**, *105*, 6888.

[36] J. C. Love, L. A. Estroff, J. K. Kriebel, R. G. Nuzzo, and G. M. Whitesides. *Chem. Rev*. **2005**, *105*, 1103.

[37] W. Azzam, C. Fuxen, A. Birkner, H. T. Rong, M. Buck, and C. Wöll. *Langmuir*. **2003**, *19*, 4958.

[38] K. Liu, X. Wang, and F. Wang. ACSNano. **2008**, *2*, 2315

[39] A. Villares, *Fabrication of molecular wires by means of the Langmuir-Blodgett and Self-Assembly Techniques.* Dissertation to obtain the degree of Doctor: University of Zaragoza, Zaragoza-Spain, **2008**.

[40] K. Bandyopadhyay, K. Vijayamohanan, M. Venkataramanan and T. Pradeep. *Langmuir*. **1999**, *15*, 5314.

[41] T. Nakamura, T. Miyamae, D. Yoshimura, N. Kobayashi, H. Nozoye, and M. Matsumoto. *Langmuir*. **2005**, *21*, 5026.

[42] T. Weidner, A. Shaporenko, J. Müller, M. Schmid, P. Cyganik, A. Terfort, and M. Zharnikov. *J. Phys. Chem. C*. **2008**, *112*, 12495.

[43] G. Pera, S. Martín, L. M. Ballesteros, A. J. Hope, P. J. Low, R. J. Nichols, and P. Cea, *Chem. Eur. J.* **2010**, *16*, 13398.

[44] A. Villares, S. Martin, I. Giner, J. Diaz, D. P. Lydon, P. J. Low, and P. Cea. *Soft Matter.* **2008**, *4*, 1508.

[45] S. Paul, C. Pearson, A. Molloy, M. A. Cousins, M. Green, S. Kolliopoulou, P. Dimitrakis, P. Normand, D. Tsoukalas, and M. C. Petty. *Nano Lett.* **2003**, *3*, 533.

[46] D. K. James, and J. M. Tour, *Chem. Mater.* **2004**, *16*, 4423.

[47] G. Pera, *Study of highly-conjugated organic compounds for the fabrication of electronic nanodevices*. Dissertation to obtain the degree of Doctor: University of Zaragoza, Zaragoza-Spain, **2011**.

[48] G. L. Gaines. *Insoluble Monolayers at Liquid-Gas Interface*. Interscience. John Wiley & Sons: New York, **1966**.

[49] L. Wilhelmy. *Annals of Physics.* **1863**, *119*, 177.

[50] M. Haro. *Estudio de Azopolímeros en películas de Langmuir-Blodgett con potenciales aplicaciones en dispositivos fotoelectrónicos.* Dissertation to obtain the degree of Doctor: University of Zaragoza, Zaragoza-Spain, **2006**.

[51] W. D. Harkins. *The Physical Chemistry of Surfaces.* Interscience: New York, **1952**.

[52] V. M. Kaganer, H. Möhwald, and P. Dutta, *Reviews of Modern Physics.* **1999**, *71*, 779.

[53] R. D. Smith, and J. C. Berg, *J. Colloid Interface Sci.* **1980**, *74*, 273.

[54] University Of Florida, *Nimet, Medical and Biological applications.* Available at: http://nimet.ufl.edu/nanomed.asp, (Accessed: 25 July 2012)

[55] W. Haiss, D. Lackey, J. K. Sass, and K. H. Besocke, *J. Chem. Phys*. **1991**, *95*, 2193.

[56] R. C. Ahuja, P. L. Caruso, D. Möbius, G. Wildburg, H. Ringsdorf, D. Philp, J. A. Preece, and J. F. Stoddart, *Langmuir*. **1993**, *9*, 1553.

[57] Jr. Oliveira, O. N. T., D. M., and H. Morgan, *Thin Solid Films.* **1992**, *210*, 76.

[58] Jr. Oliveira, O. N. B., C. *Langmuir*. **1997**, *13*, 5920.

[59] G. Sauerbrey, *Zeitschrift fur Physik.* **1959**, *155*, 206.

[60] S. C., J. T. Rubin, J. P. Ferrais, and T. A. Zawodzinski, *Langmuir.* **1996**, *12*, 363.

[61] J. S., K. Yoshida, J. Kameda, H. Sato, A. Yamagishi, L. Sun, M. Corriea, and G. Villemure, *Langmuir*. **2006**, *22*, 9591.

[62] R.U. Ugas, *Investigation of Stabilizing Agents in Thin Sol-Gel Zirconium Oxide Anti-corrosion Coatings on Iron Materials*. Dissertation to obtain the degree of Doctor: TU-Darmstadt University, Germany, **2010**.

[63] P. Cea, M. C. López, S. Martín, A. Villares, G. Pera, and I. Giner, *J. Chem. Educ.* **2009**, *86*, 723.

[64] M. S.-H., N. Brust, K. Norgaard, J. B. Christensen, L. K. Nielsen, and T. Bjornholm, *Nano Letters.* **2001**, *1*, 189.

[65] A. Villares, S. Martín, R. J. Nichols, D. P. Lydon, L. Applegarth, A. Beeby, P. J. Low, and P. Cea, *Chem. Mater*. **2010**, *22*, 2041.

[66] Amsterdam University, *Viral mechanics, AFM schematics.* Available at: http://www.few.vu.nl/~wroos/Virus.html, (Accessed: 18 July 2012)

[67] J. Moreland, and J. W. Ekin, *J. Appl. Phys*. **1985**, *58*, 3888.

[68] B. Q. Xu, and N. J. J. Tao, *Science.* **2003**, *301*, 1221.

[69] W. Haiss, H. van Zalinge, S. J. Higgins, D. Bethell, H. Hobenreich, D. J. Schiffrin, and R. J. Nichols, *J. Am. Chem. Soc.* **2003**, *125*, 15294.

[70] T. J. C., P. M. Halthur, and U. M. Elofsson, *Langmuir.* **2006**, *22*, 11065.

[71] G. Pera, A. Villares, Mª C. López, P. Cea, D. P. Lydon, and P. J. Low, *Chem. Mater*. **2007**, *19*, 857.

[72] A. Villares, D. P. Lydon, L. Porrès, A. Beeby, P. J. Low, P. Cea, and F. M. Royo, *J. Phys. Chem. B.* **2007**, *111*, 7201.

[73] A. Villares, D. P. Lydon, P. J. Low, B. J. Robinson, G. J. Ashwell, F. M. Royo, and P. Cea, *Chem. Mater.* **2008**, *20*, 258.

[74] M. Haro, B. Giner, C. Lafuente, M. C. López, F. M. Royo, and P. Cea, *Langmuir*. **2005**, *21*, 2796.

[75] V. Tsoukanova, and C. Salesse, *Langmuir.* **2008**, *24*, 13019.

[76] G. L. Xu, M. C. DeRosa, R. J. Crutchley, and T. Ren, *J. Am. Chem. Soc.* **2004**, *126*, 3728.

[77] Q. Lu, K. Liu, H. Zhang, Z. Du, X. Wang, and F. Wang, *ACS Nano*. **2009**, *3*, 3861.